Mon. Not. R. Astron. Soc. **000**, 000–000 (0000) Printed 18 May 2016 (MN LATEX style file v2.2)

# Boundary between Stable and Unstable Regimes of Accretion. Ordered and Chaotic Unstable Regimes

A. A. Blinova*, M. M. Romanova†, R.V.E. Lovelace‡
*Dept. of Astronomy, Cornell University, Ithaca, NY 14853*

18 May 2016

arXiv:1501.01948v2 [astro-ph.SR] 16 May 2016

**ABSTRACT**

We present a new study of the Rayleigh-Taylor unstable regime of accretion onto rotating magnetized stars in a set of high grid resolution three-dimensional (3D) magnetohydrodynamic (MHD) simulations performed in low-viscosity discs. We find that the boundary between the stable and unstable regimes is determined almost entirely by the fastness parameter $\omega_s = \Omega_\star/\Omega_K(r_m)$, where $\Omega_\star$ is the angular velocity of the star and $\Omega_K(r_m)$ is the angular velocity of the Keplerian disc at the disc-magnetosphere boundary $r = r_m$. We found that accretion is unstable if $\omega_s \lesssim 0.6$. Accretion through instabilities is present in stars with different magnetospheric sizes. However, only in stars with relatively small magnetospheres, $r_m/R_\star \lesssim 7$, do the unstable tongues produce chaotic hot spots on the stellar surface and irregular light-curves. At even smaller values of the fastness parameter, $\omega_s \lesssim 0.45$, multiple irregular tongues merge, forming one or two *ordered unstable* tongues that rotate with the angular frequency of the inner disc. This transition occurs in stars with even smaller magnetospheres, $r_m/R_\star \lesssim 4.2$. Most of our simulations were performed at a small tilt of the dipole magnetosphere, $\Theta = 5^\circ$, and a small viscosity parameter $\alpha = 0.02$. Test simulations at higher $\alpha$ values show that many more cases become unstable, and the light-curves become even more irregular. Test simulations at larger tilts of the dipole $\Theta$ show that instability is present, however, accretion in two funnel streams dominates if $\Theta \gtrsim 15^\circ$. The results of these simulations can be applied to accreting magnetized stars with relatively small magnetospheres: Classical T Tauri stars, accreting millisecond X-ray pulsars, and cataclysmics variables.

**Key words:** accretion, accretion discs; MHD; stars: neutron; stars: magnetic fields

## 1 INTRODUCTION

Magnetospheric accretion occurs in different types of stars, including Classical T Tauri stars (CTTSs) (e.g., Bouvier et al. 2007), magnetized cataclysmic variables (CVs) (e.g., Warner et al. 1995; Hellier 2001), and accreting millisecond X-ray pulsars (AMXPs)(e.g., van der Klis 2006). The dynamically-important magnetic field stops the accretion disc at some distance from the star, $r_m$ (called the magnetospheric radius), and subsequently, the magnetic field governs the flow of matter onto the star (e.g., Pringle & Rees 1972; Ghosh & Lamb 1978; Campbell 1992; Lovelace et al. 1995).

The disc-magnetosphere boundary is prone to the Kelvin-Helmholtz and magnetic Rayleigh-Taylor (RT) instabilities (e.g., Chandrasekhar 1961, Arons & Lea 1976). It was suggested in earlier studies that the instabilities at the disc-magnetosphere boundary may only lead to the mixing of plasma with the field in the external layers of the magnetosphere (Arons & Lea 1976). However, our global 3D MHD simulations show that the disc matter can deeply penetrate the magnetosphere in tongues which produce chaotic hot spots on the stellar surface and irregular light-curves. Simulations show that matter may accrete in either the stable or the unstable regime. In the stable regime, matter is lifted above the magnetosphere and accretes in two ordered funnel streams, forming two ordered hot spots on the surface of the star (Romanova et al. 2003, 2004; Kulkarni & Romanova 2005). In the unstable regime, matter penetrates through the magnetosphere in several equatorial "tongues" due to the magnetic Rayleigh-Taylor instability and forms several chaotic spots on the surface of the star (Kulkarni & Romanova 2008; Romanova et al. 2008; Bachetti et al. 2010; Kurosawa & Romanova 2013). The light-curves associated with the hot spots are expected to be periodic in the stable regime, and irregu-

* E-mail: alisablinova@gmail.com
† E-mail: romanova@astro.cornell.edu
‡ E-mail: lovelace@astro.cornell.edu

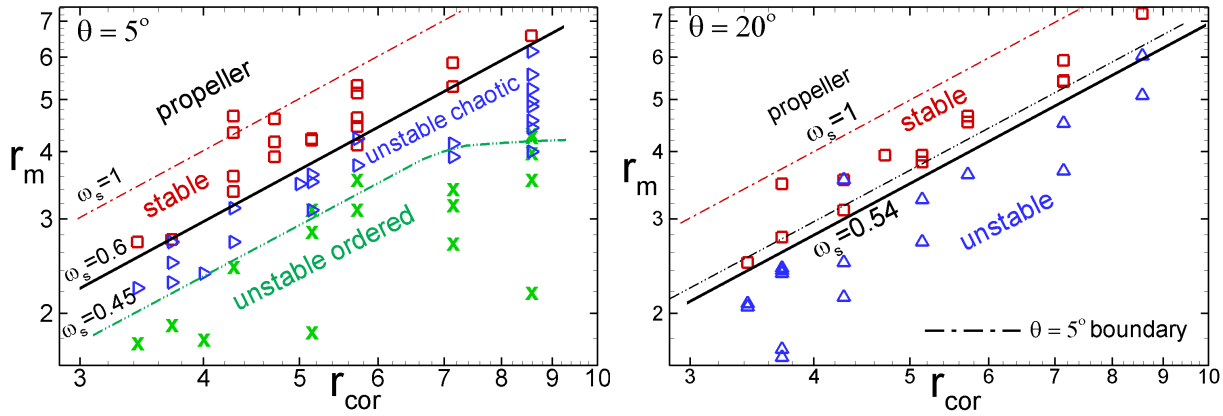



**Figure 1.** The boundary between stable and unstable regimes of accretion in the parameter space of $r_m$ and $r_{\rm cor}$ for two different misalignment angles of the dipole: $\theta = 5^\circ$ and $\theta = 20^\circ$. Here, the units of length are given in stellar radii for user convenience. *Left panel*: boundary line for $\Theta = 5^\circ$. Stable, chaotic unstable, and ordered unstable accretion cases are represented by red squares, blue triangles, and green x's, respectively. *Right panel*: the boundary between stable and unstable regimes for $\Theta = 20^\circ$. The dash-dot-dot line shows the boundary for $\theta = 5^\circ$.

lar in the unstable regime, with a typical time-scale of a few peaks per rotational period of the inner disc.

Simulations performed locally in the 3D simulation box also show that an ordered magnetic field is not an obstacle for the magnetic Rayleigh-Taylor instability (e.g., Rastätter & Schindler 1999; Stone & Gardiner 2007a,b). These simulations and earlier simulations by Wang & Robertson (1984, 1985) show that the Rayleigh-Taylor instability leads to the formation of small-scale waves and filaments that merge to form much larger filaments, which then deeply penetrate the magnetically-dominated, low-density regions.

The possible importance of the model for understanding CTTSs as well as other magnetized stars (such as AMXPs and IPs) pushed us to reconsider the unstable regime with new, more advanced simulations at a higher grid resolution. Test simulations showed that accretion through instabilities appeared in many more cases, including those which were stable in simulations with the coarser grid. For example, in the former simulations, accretion was usually stable in the cases of a small $\alpha-$parameter of viscosity (Shakura & Sunyaev 1973). However, in the new simulations, many of these cases become unstable. We concluded that the coarse grid was a factor that suppressed or weakened instability in many of our earlier simulations, so we reconsidered the problem using a higher grid resolution. We also tested the convergence of the code at several grids with increasing resolutions.

One of the important questions is, what determines the boundary between stable and unstable regimes of accretion? In prior work, we derived an empirical boundary that was based on the accretion rate (which we varied using the $\alpha-$parameter of viscosity, e.g. Romanova et al. 2008). This boundary was useful, although it has not been completely understood. This prior work led to the important conclusion that models with higher values of $\alpha$ are more unstable. One of the goals of our current research is to derive a boundary between stable and unstable regimes at a low viscosity in the disk.

Another important phenomenon that has been systematically observed in the new simulations is the frequent presence of what we call the *ordered unstable regime*, where the unstable tongues merge to form one or two "ordered" tongues that rotate with the frequency of the inner disc. The accretion in ordered unstable regime has been observed in earlier simulations (performed at a lower grid resolution), but only in the cases of very small magnetospheres and high $\alpha-$parameters (Romanova & Kulkarni 2009). In recent simulations at a higher grid resolution, we observed that this regime is present at a wider range of parameter values, including larger-sized magnetospheres and lower viscosities in the disc.

In this paper, we focus on two main issues: (1) searching a new boundary between the stable and unstable regimes; (2) investigating the ordered unstable regime and finding a boundary between the ordered and chaotic unstable regimes.

In Sec. 2 we discuss the theoretical background of the problem. In Sec. 3 we describe the numerical model used in our simulations. In Sec. 4 we search for the boundary between stable and unstable regimes of accretion. In Sec. 5 we describe the ordered and chaotic regimes of unstable accretion, and derive the boundary between them. In Sec. 6 we analyze instability and investigate the dependence of instability on the corotation radius and the $\alpha-$parameter of viscosity. In Sec. 7 we investigate the grid convergence of the model. In Sec. 8 we discuss the properties of accretion through instabilities in the cases of larger tilts of the dipole, $\Theta$. In Sec. 9 we compare relativistic and non-relativistic cases. In Sec. 10 we discuss the applications to different magnetized stars. We conclude in Sec. 11.

## 2 THEORETICAL BACKGROUND

### 2.1 Disk-magnetosphere boundary.

The magnetic field of the star truncates the accretion disk at a radius $r_m$ where the magnetic stress in the magnetosphere matches the matter stress in the disk (e.g., Pringle & Rees 1972; Lamb et al. 1973):

$$p + \rho v^2 = B^2/8\pi, \quad \text{or} \quad \beta_1 = 8\pi(p + \rho v^2)/B^2 = 1\,, \qquad (1)$$

where $\rho$, $p$, $v$ and $B$ are the local density, gas pressure, velocity and magnetic field, respectively. Here, $\beta_1$ is the generalized plasma parameter, which includes both *thermal and ram pressure* (Romanova et al. 2002). It is analogous to the

| Model | $\mu$ | $r_{\rm cor}$ | $\alpha$ | $\Theta$ | $P_\star$ | $P_{\rm inst}$ | Comments |
|---|---|---|---|---|---|---|---|
| $\mu 0.3 c 1.8 \Theta 5 \alpha 0.02$ | 0.3 | 1.8 | 0.02 | 5 | 2.4 | 1.5 | intermediate (unstable chaotic/stable) |
| $\mu 0.3 c 2.5 \Theta 5 \alpha 0.02$ | 0.3 | 2.5 | 0.02 | 5 | 3.9 | 1.9 | unstable ordered |
| $\mu 0.3 c 5 \Theta 10 \alpha 0.02$ | 0.3 | 5 | 0.02 | 10 | 11.2 | 2.2 | unstable ordered/chaotic |
| $\mu 0.5 c 1.5 \Theta 5 \alpha 0.02$ | 0.5 | 1.5 | 0.02 | 5 | 1.8 | 0.9 | unstable chaotic |
| $\mu 0.5 c 2 \Theta 5 \alpha 0.02$ | 0.5 | 2 | 0.02 | 5 | 2.8 | 2.4 | unstable chaotic |
| $\mu 0.5 c 3 \Theta 5 \alpha 0.02$ | 0.5 | 3 | 0.02 | 5 | 5.2 | 2.3, 2.7 | unstable ordered/chaotic |
| $\mu 0.5 c 5 \Theta 5 \alpha 0.02$ | 0.5 | 5 | 0.02 | 5 | 11.2 | 3 | unstable ordered |
| $\mu 0.5 c 3 \Theta 5 \alpha 0.1$ | 0.5 | 3 | 0.1 | 5 | 5.2 | 1.6 | unstable chaotic |
| $\mu 0.5 c 5 \Theta 5 \alpha 0.1$ | 0.5 | 5 | 0.1 | 5 | 11.2 | 2.6 | unstable ordered |
| $\mu 0.5 c 3 \Theta 20 \alpha 0.02$ | 0.5 | 3 | 0.02 | 20 | 5.2 | 1.9, 2.7 | unstable chaotic/ordered |
| $\mu 1 c 1.8 \Theta 5 \alpha 0.02$ | 1 | 1.8 | 0.02 | 5 | 2.4 | 0.85 | intermediate (unstable chaotic/stable) |
| $\mu 1 c 2 \Theta 5 \alpha 0.02$ | 1 | 2 | 0.02 | 5 | 2.8 | 0.4-1.6 | intermediate (unstable chaotic/stable) |
| $\mu 1 c 2.5 \Theta 5 \alpha 0.02$ | 1 | 2.5 | 0.02 | 5 | 3.9 | 3 | unstable chaotic |
| $\mu 1 c 3 \Theta 5 \alpha 0.02$ | 1 | 3 | 0.02 | 5 | 5.2 | 1.9, 3.8 | unstable ordered |
| $\mu 1 c 5 \Theta 5 \alpha 0.02$ | 1 | 5 | 0.02 | 5 | 11.2 | 1.8, 7.4 | unstable ordered |
| $\mu 1 c 1.5 \Theta 5 \alpha 0.1$ | 1 | 1.5 | 0.1 | 5 | 1.8 | 0.9 | unstable chaotic |
| $\mu 1 c 3 \Theta 5 \alpha 0.1$ | 1 | 3 | 0.1 | 5 | 5.2 | 2.7 | unstable chaotic |
| $\mu 2 c 2 \Theta 5 \alpha 0.02$ | 2 | 2 | 0.02 | 5 | 5.2 | 2.8 | stable |
| $\mu 2 c 3 \Theta 5 \alpha 0.02$ | 2 | 3 | 0.02 | 5 | 5.2 | 2.8 | unstable chaotic |

**Table 1.** Sample (representative) models for different values of parameters $\mu$, $r_{\rm cor}$, $\alpha$, and $\Theta$. The period of the star $P_\star$ and the periods of instabilities $P_{\rm inst}$ obtained in Fourier spectral analysis are shown.

standard plasma parameter $\beta = 8\pi p/B^2$, but takes into account the ram pressure of the matter flow in the disk. Axisymmetric and global 3D MHD simulations show that the condition $\beta_1 = 1$ is valuable for finding the magnetospheric radius $r_m$ (e.g., Kulkarni & Romanova 2013). This radius $r_m$ corresponds to the innermost edge of the disk, where the density drops sharply towards the low-density magnetosphere. This formula can be used to find $r_m$ in many situations, including those that are non-stationary or where the magnetic field is more complex than the dipole one. Sometimes, the condition $\beta = 8\pi p/B^2 = 1$ is used to find the magnetospheric radius (e.g., Bessolaz et al. 2008). This condition, however, yields a somewhat larger radius at which matter flows from the disk to the funnel stream.

In theoretical studies (e.g., Pringle & Rees 1972; Lamb et al. 1973) the magnetospheric radius was estimated from the balance between the largest components of the stresses, assuming a dipole field of the star and Keplerian orbital speed in the disk; this gives

$$r_m = k\big[\mu_\star^4/(\dot{M}^2 G M_\star)\big]^{1/7}, \quad k \sim 1\ , \tag{2}$$

where $\mu_\star = B_\star R_\star^3$ is the magnetic moment of the star with a surface field $B_\star$, $\dot{M}$ is the disk accretion rate, and $M_\star$ and $R_\star$ are the mass and radius of the star, respectively.

Axisymmetric simulations by, e.g., Long et al. (2005) found that eqs. 1 and 2 give similar values of $r_m$ if $k \approx 0.5$. Kulkarni & Romanova (2013) performed a series of 3D MHD simulations of accretion in the stable regime and compared theoretically-derived values of $r_m$ (using Eq. 2) with those obtained from simulations (using condition $\beta_1 = 1$). They found that, in the range of magnetospheric radii $r_m \sim (2-5)R_\star$, the radius $r_m$ obtained from the simulations can be described by Eq. 2 if $0.55 \lesssim k \lesssim 0.72$. Here, we performed similar comparisons between numerically-derived magnetospheric radii and Eq. 2 using numerical runs in the stable and unstable regimes (see Appendix A).

Another important radius is the corotation radius, $r_{\rm cor}$, where, by definition, the angular velocity of the star matches the Keplerian angular velocity of the disc: $\Omega_\star = \sqrt{GM_\star/r_{\rm cor}^3}$, from which we obtain $r_{\rm cor} = [GM_\star/{\Omega_\star}^2]^{1/3}$. Both the magnetospheric radius $r_m$ and corotation radius $r_{\rm cor}$ are useful in the analysis of magnetized stars.

Another convenient parameter that is often used while investigating the physics at the disk-magnetosphere boundary is the fastness parameter, which is the ratio between the angular velocity of the star and the Keplerian angular velocity at the disk-magnetosphere boundary $r = r_m$ (e.g., Ghosh & Lamb 1978; Ghosh 2007):

$$\omega_s = \frac{\Omega_\star}{\Omega_K(r_m)}\ , \qquad \text{or,} \qquad \omega_s = \left(\frac{r_m}{r_{\rm cor}}\right)^{3/2}. \tag{3}$$

One can see that this parameter is also a simple function of the ratio between two main radii, $r_m$ and $r_{\rm cor}$. The fastness parameter $\omega_s$ is expected to be significant in determining the processes at the disk-magnetosphere boundary (e.g., Ghosh 2007). In our study we use either $\omega_s$ or the ratio $r_m/r_{\rm cor}$.

### 2.2 Rayleigh-Taylor instability at the disk-magnetosphere boundary

The disk-magnetsophere boundary is prone to Rayleigh-Taylor and Kelvin-Helmholtz instabilities. Detailed simulations of the boundary in the shearing box (Rastätter & Schindler 1999) and also global simulations (e.g., Kulkarni & Romanova 2008) show that the RT instability strongly dominates. In a simplified case of two adjacent, rotating inviscid fluids with the magnetic field perpendicular to the boundary between them, the boundary is unstable if the effective gravity $g_{\rm eff} = g + g_c$ is negative (Chandrasekhar 1961). Here, $g = -GM_\star/r^2$ and $g_c = {\Omega_\star}^2 r$ are gravitational and centrifugal acceleration, respectively. Taking into account that at

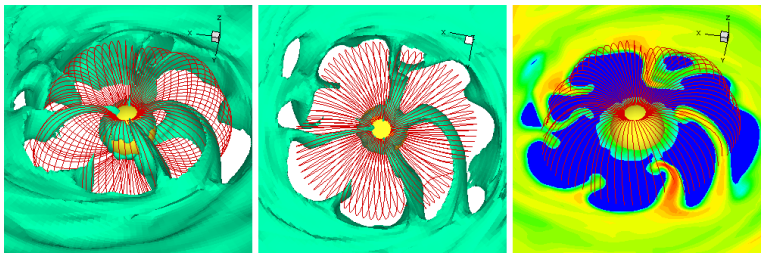


**Figure 2.** *Left panel*: 3D view of matter flow in a case where chaotic accretion in multiple tongues dominates, model $\mu 1c2.5\Theta 5a0.02$, at time $t = 19$. One of the density levels is shown in color, selected magnetic field lines are shown in red. *Middle panel*: Same but in the face-on projection. *Right panel:* An equatorial slice of density distribution is shown in color.

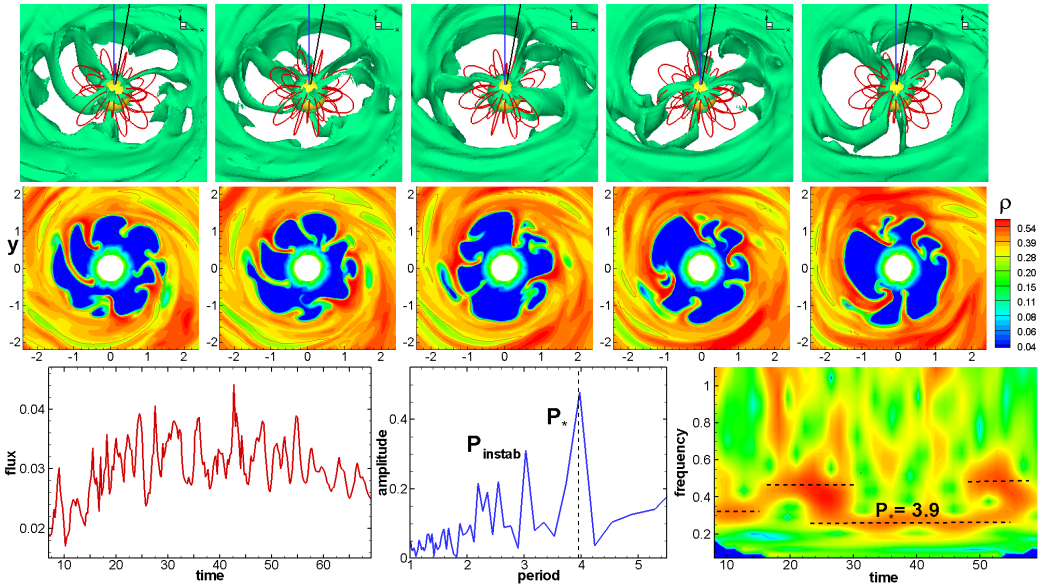



**Figure 3.** An example of accretion in the chaotic unstable regime in the model $\mu 1c2.5\Theta 5\alpha 0.02$ (times $t = 19 - 21$), where multiple tongues form. Top row shows consecutive 3D views of matter flow, where the color background represents one of the density levels and the lines are sample magnetic field lines. The axes show the directions for the angular momentum and magnetic momentum of the star. The middle panel shows consecutive xy slices. The color background shows density distribution and the lines show where the kinetic plasma parameter $\beta_1 = 1$. Bottom row shows the light-curve from rotating spots calculated at an inclination angle $i = 45^\circ$ (left panel), Fourier transform (middle panel) and wavelet transform (right panel) obtained from analysis of the light-curve.

the boundary ($r = r_m$) $g = -GM_\star/r^2 = -\Omega_K^2 r$, where $\Omega_K = \sqrt{GM_\star/r_m^3}$ is the Keplerian velocity at the disc-magnetosphere boundary, we obtain

$$g_{\rm eff} = -\Omega_K^2 r + {\Omega_\star}^2 r = -\Omega_K^2 r(1-\omega_s^2). \quad (4)$$

One can see that in this simplified case the boundary is unstable , *if* $\omega_s < 1$.

A more detailed theoretical analysis shows that in a realistic situation there are a number of factors that can suppress instability. One of these factors is viscosity in the disc. This viscosity may be associated with the turbulence in the disk. Alternatively, it can be numerical viscosity associated with the finite size of the grid in numerical models. Both types of viscosity can suppress the short wavelength perturbations (Chandrasekhar 1961). On the other hand, the azimuthal component of the field $B_\phi$ can also suppress the short-wavelength perturbation modes (Chandrasekhar 1961). In addition to the above factors, the differential rotation of matter in the disk, $d\Omega/dr$, tends to suppress the RT unstable modes (e.g., Kaisig et al. 1992).

Another important factor that can increase or decrease the strength of instability is the compression factor $K_{\rm B\Sigma} = \left|\frac{d}{dr}\ln\frac{\Sigma}{B_z}\right|$, which is the gradient of surface density per unit of magnetic flux. The growth rate of the RT instability is larger if the gradient of $\Sigma/B_z$ increases fast enough in the direction of gravity (Kaisig et al. 1992; Lubow & Spruit 1995).

Spruit et al. (1995) have performed a general analysis of disc stability in the thin disc approximation, taking the velocity shear into account The disc has a surface density $\Sigma$ and is threaded by a magnetic field with the vertical component $B_z$. Their analytical criterion for the development of instability is:

$$\gamma_{B\Sigma}^2 \equiv (-g_{\rm eff})\left|\frac{d}{dr}\ln\frac{\Sigma}{B_z}\right| > 2\left(r\frac{d\Omega}{dr}\right)^2 \equiv \gamma_\Omega^2\,. \quad (5)$$

One can see that large, negative values of effective gravitational acceleration $g_{\rm eff}$ and large values of the compression factor $K_{\rm B\Sigma} = \left|\frac{d}{dr}\ln\frac{\Sigma}{B_z}\right|$ lead to stronger instability, while the radial shear, $\gamma_\Omega^2 = 2\left(r\frac{d\Omega}{dr}\right)^2$, is a factor that suppresses

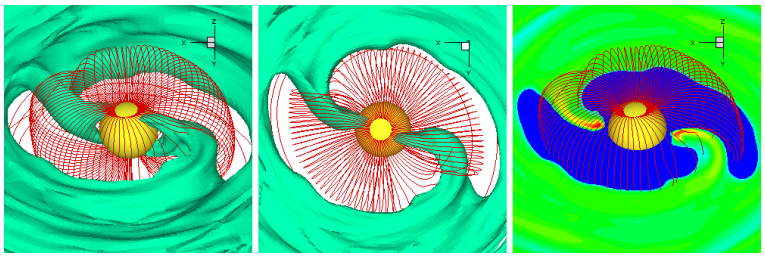


**Figure 4.** *Left panel*: Same as Fig. 2, but for a case where ordered accretion in two tongues dominates, model $\mu 0.5c3\Theta 5a0.02$, at time $t = 14$.

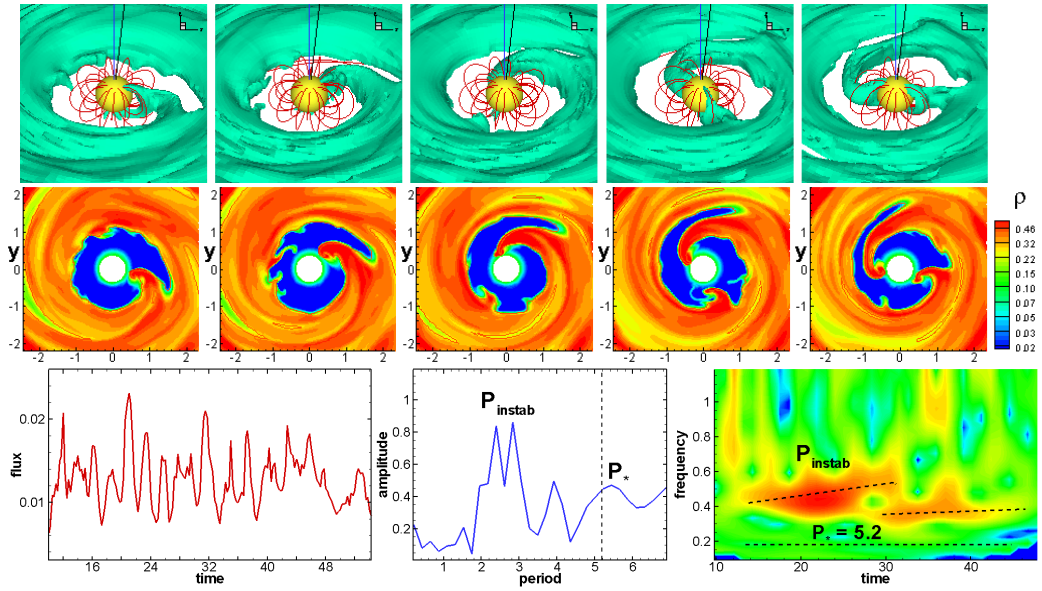



**Figure 5.** Same as Fig. 3, but for accretion in the ordered unstable regime, model $\mu 0.5c3\Theta 5\alpha 0.02$ (times $t = 25.5 - 27.5$), where one or two ordered unstable tongues form.

instability by smearing out the perturbations. This criterion is valuable for the analysis of the disk-magnetosphere boundary. However, it does not take into account the possible suppression of perturbation modes by the azimuthal field, $B_\phi$, or by viscosity. Global 3D MHD simulations are required to take into account all of these factors, provided that the grid resolution is fine enough to resolve (and not suppress) the small-scale perturbation modes.

## 3 NUMERICAL MODEL

We perform global 3D MHD simulations of disc accretion onto a rotating magnetized star. The model we use is the same as in our earlier 3D MHD simulations of stable and unstable regimes (e.g., Romanova et al. 2008; Kulkarni & Romanova 2008), which has been described in our earlier papers (e.g., Koldoba et al. 2002; Romanova et al. 2003). Hence, we will only describe it briefly here.

### 3.1 Initial and boundary conditions

*Initial conditions.* A star has a dipole magnetic moment $\mu$, the axis of which makes an angle $\Theta$ with the star's rotational axis $\Omega_\star$. The rotational axes of the star and the accretion disc are aligned. A star is surrounded by an accretion disc and a corona. The disc is cold and dense, while the corona is hot and rarefied, and at the reference point (the inner edge of the disc in the disc plane) the temperature and density are $T_c = 100T_d$, and $\rho_c = 0.01\rho_d$, where subscripts 'd' and 'c' denote the disc and the corona. Initially, the disc and corona are in rotational hydrodynamic equilibrium (see e.g., Romanova et al. 2002 for details). The disc is relatively thin, with the half-thickness to radius ratio $h/r \approx 0.1$.

*Boundary conditions.* At both the inner and outer boundaries, most of the variables $A_j$ are taken to have free boundary conditions, $\partial A_j/\partial r = 0$. The free boundary conditions on the hydrodynamic variables at the stellar surface mean that accreting gas can cross the surface of the star without creating a disturbance in the flow. These conditions neglect the complex physics of interaction between the accreting gas and the star [1]. The magnetic field is frozen onto the surface of the star. That is, the normal component of the field, $B_n$, is fixed. The other components of the magnetic field vary. At the outer boundary, matter is not permitted to flow into the region. The simulation region is usually large enough for the disc to have

[1] The impact of accreting matter with the stellar surface and formation of the radiative shock wave near the surface has been investigated, e.g., by Koldoba et al. (2008); Orlando et al. (2010).

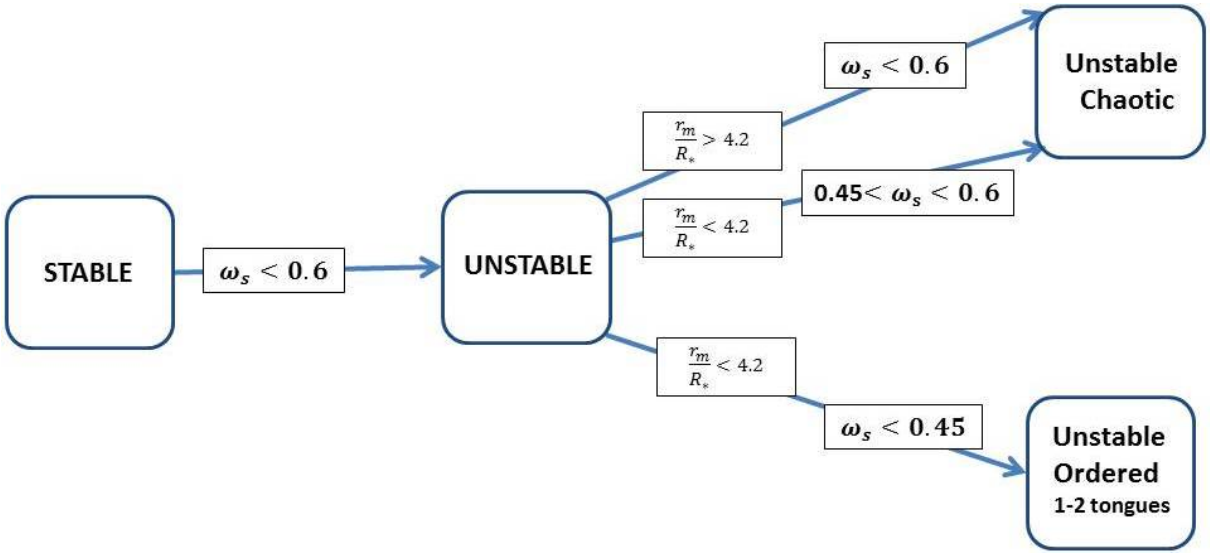



**Figure 6.** The diagram shows transitions between stable and two types of unstable regimes discussed in the paper and calculated for low viscosity, $\alpha = 0.02$, and a small tilt of the dipole magnetosphere, $\Theta = 5^\circ$. The diagram shows the dependence of boundaries on the fastness parameter $\omega_s$. The ratio $r_m/R_\star$ shows the dimensionless size of the magnetosphere at which chaotic or ordered type of instability have been observed.

enough mass to sustain accretion flow for the duration of the simulation run.

### 3.2 MHD equations, numerical method and the grid

The full set of 3D MHD equations taken in dimensionless form is solved numerically using a Godunov-type numerical scheme, written in a "cubed-sphere" coordinate system which rotates with the star (Koldoba et al. 2002). The numerical approach is similar to that described in Powell (1999), where the seven wave Roe-type approximate Riemann solver is used. The energy equation is written in the form of entropy balance, and the equation of state is that of an ideal gas. Compared with Koldoba et al. (2002), viscosity terms are incorporated into the equations. Viscosity is modelled using the $\alpha$-model (Shakura & Sunyaev 1973), and is incorporated only into the disc, so that it controls the accretion rate through the disc. In contrast with our earlier studies, we use a small $\alpha$-parameter $\alpha = 0.02$ in most of the simulation runs, and use a larger value $\alpha = 0.1$ in the test runs.

A "cubed sphere" grid consists of $N_r$ concentric spheres, where each sphere represents an inflated cube. Each of the six sides of the inflated cube has an $N \times N$ curvilinear grids which represent a projection of the Cartesian grid onto the sphere. The entire grid consists of $6N^2 \times N_r$ cells. The typical grid used in our simulations has $N_r = 140$ cells in the radial direction, and $N^2 = 61^2$ *'angular'* cells in each block. This grid is twice as fine as the $N^2 = 31^2$ grid used in our earlier studies of instabilities (e.g., Kulkarni & Romanova 2008). To check the convergence of results at higher grid resolutions, the following grids were also calculated: $51^2 \times 110$, $71^2 \times 160$, $81^2 \times 185$, and $101^2 \times 220$. Simulations show that at a small parameter of viscosity ($\alpha = 0.02$) the coarsest grid, $31^2$, suppresses instability, while at all finer grids the results do not depend on the grid resolution (see details in Sec. 6).

### 3.3 Dimensionalization

Equations are written using *dimensionless variables*. The dimensionless value of every physical quantity $A_j$ is defined as $\tilde{A}_j = A_j/A_{j0}$, where $A_{j0}$ is the reference value for $A_j$. The simulations were performed in dimensionless variables $\widetilde{A}$.

First, we define the main reference values: the reference scale, $R_0 = R_\star/0.35$, where $R_\star$ is the radius of the star [2]; the reference mass, $M_0 = M_\star$, where $M_\star$ is the mass of the star; and the magnetic moment of the star, $\mu_\star = B_\star R_\star^3$, where $B_\star$ is the magnetic field at the magnetic equator. Then, we determine the other reference values, which include: velocity $v_0 = (GM_0/R_0)^{1/2}$; time-scale $t_0 = R_0/v_0$; period of rotation at $r = R_0$: $P_0 = 2\pi R_0/v_0$ ( used in our plots); reference angular velocity $\Omega_0 = v_0/R_0$; and reference frequency $f_0 = \Omega_0/2\pi$. We determine the reference magnetic field $B_0$ and magnetic moment $\mu_0 = B_0 R_0^3$ such that $\mu_0 = \mu_\star/\widetilde{\mu}$, where $\widetilde{\mu}$ is the dimensionless parameter used to vary the size of the dimensionless magnetosphere. The reference field is $B_0 = \mu_\star/(R_0^3\widetilde{\mu})$, the reference density is $\rho_0 = B_0^2/v_0^2$, the reference mass accretion rate is $\dot{M}_0 = \rho_0 v_0 R_0^2 = \mu_\star^2/(\widetilde{\mu}^2 R_0^4 v_0)$, and the reference surface density is $\Sigma_0 = \rho_0 R_0$.

The results obtained in dimensionless variables $\widetilde{A}$ can be applied to different types of stars. We determine the dimensional mass, radius and magnetic field of a star and derive other reference values, as discussed above. Table B lists the reference values for three classes of stars: classical T Tauri stars, white dwarfs and neutron stars. To obtain the physical dimensional values $A$, the dimensionless values $\widetilde{A}$ should be multiplied by the corresponding reference values $A_0$ as $A = \widetilde{A}A_0$. Subsequently, in the text we drop the tildes above the dimensionless variables and show dimensionless values everywhere unless otherwise specified.

[2] This reference scale has been used in our prior models (e.g., Koldoba et al. 2002; Romanova et al. 2002), and we now use it for consistency with our earlier works.

### 3.4 Main dimensionless parameters of the model.

Taking into account the above dimensionalization, the number of parameters in the problem is relatively small. The dimensionless mass and radius of the star, $\tilde{M}_\star = 1$ and $\tilde{R}_\star = 0.35$, respectively, are fixed throughout all simulation runs. We fix the fiducial density values in the disk and corona at $\tilde{\rho}_d = 1$ and $\tilde{\rho}_c = 0.01$, respectively, and use the same disk structure across all simulation runs. The only parameter that is varied is the $\alpha-$parameter of viscosity, which regulates the radial velocity in the disk, $v_r \sim \alpha$ (Shakura & Sunyaev 1973). We use a small $\alpha-$parameter, $\alpha = 0.02$, in most simulation runs.

There are two main dimensionless parameters that we vary. One of them is the dimensionless corotation radius $\tilde{r}_{\rm cor}$, which determines the dimensionless angular velocity of the star, $\tilde{\Omega}_\star = \tilde{r}_{\rm cor}^{-3/2}$. This is one of the key parameters in determining the boundary between stable and unstable regimes of accretion.

The second important parameter is the dimensionless magnetic moment $\widetilde{\mu}$, which determines the size of the dimensionless magnetosphere, $\widetilde{r}_m = r_m/R_0$. We do not know the size of the magnetosphere in advance. Instead, we obtain it from the simulations. We can estimate the expected size of the magnetosphere using the theoretical formula Eq. 2 and substituting the magnetic moment of the star, $\mu_\star$, with that obtained from our dimensionalization formalism: $\dot{M}_0 = \mu_\star^2/(\widetilde{\mu}^2 R_0^4 v_0)$, or $\mu_\star^2 = \dot{M}_0 \widetilde{\mu}^2 R_0^4 v_0$ and $v_0 = (GM/R_0)^{1/2}$. We obtain:

$$\widetilde{r}_m = r_m/R_0 = k(\widetilde{\mu}^2/\widetilde{\dot{M}})^{2/7} \ . \qquad (6)$$

Here, $\widetilde{\dot{M}}$ is the dimensionless accretion rate, which we find from simulations and typically does not vary much across simulations with similar $\alpha-$parameters of viscosity. The main parameter that determines the dimensionless size of the magnetosphere, $r_m/R_\star$, is parameter $\widetilde{\mu}$. These two parameters ($\widetilde{r}_{\rm cor}$ and $\widetilde{\mu}$) determine the main physics at the disk-magnetosphere boundary [3]. In the following sections, we drop the tilde's above $\widetilde{\mu}$ and $\widetilde{r}_{\rm cor}$ for convenience.

The results also depend on the tilt of the dipole magnetosphere, $\Theta$. We investigated the cases of small ($\Theta = 5^\circ$) and larger ($\Theta \geq 20^\circ$) tilts in separate sets of runs.

## 4 BOUNDARY BETWEEN STABLE AND UNSTABLE REGIMES OF ACCRETION

One of the main goals of present research was to find a set of parameters which would determine the boundary between stable and unstable regimes of accretion.

### 4.1 Set of performed simulations

To find the boundary between stable and unstable regimes of accretion, we performed a series of simulation runs, where we kept the same initial conditions for the density and pressure distribution in the disc and corona, but varied the the main dimensionless parameters of the model: magnetic moment $\mu$ of the star (which determines the dimensionless size of the magnetosphere) and the corotation radius $r_{\rm cor}$ (which determines the period of the star). We used a small parameter of viscosity, $\alpha = 0.02$, in the majority of simulation runs to be sure that viscosity is not an essential factor in generating or suppressing instability.

We ran two main sets of simulations for two different misalignment angles of the dipole moment: one at a relatively small angle, $\Theta = 5^\circ$, where instability is expected to be stronger, and the other at a larger angle, $\Theta = 20^\circ$, where funnel stream accretion is expected to be more favorable (e.g., Kulkarni & Romanova 2008).

For each angle $\Theta$, we performed a series of simulations for stars with different corotation radii in the range of $r_{\rm cor} = 1.2 - 5$ and parameters $\mu$ ranging from $\mu = 0.1$ (small-sized magnetospheres) to $\mu = 3$ (large-sized magnetospheres). Table 1 shows sample models used for finding the boundary. Many of these models were also used for detailed analysis. The names of the models in the Table incorporate the parameters used in those models.

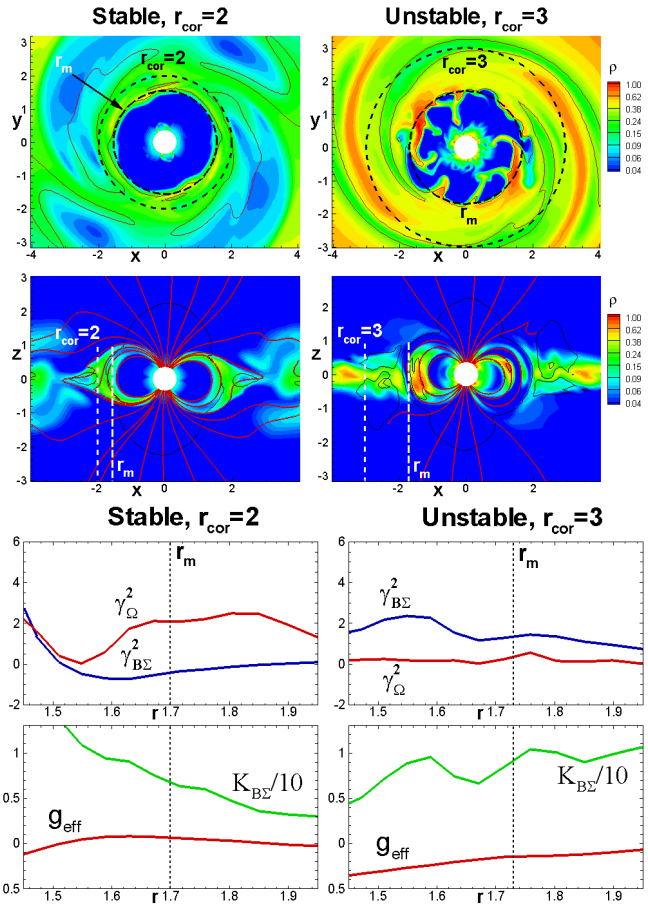



**Figure 7.** *Top four panels:* Example of two simulation runs with same parameters ($\mu = 2$, $\Theta = 5^\circ$, $\alpha = 0.02$ at time $t = 20$) but different corotation radii (models $\mu 2c2\Theta 5\alpha 0.02$ and $\mu 2c3\Theta 5\alpha 0.02$). *Left panels*: xy-slice (top) and xz-slice (bottom) show the density distribution in case of $r_{\rm cor} = 2$, where accretion is stable. *Right panels*: accretion becomes unstable when $r_{\rm cor} = 3$. Red lines show sample magnetic field lines. Positions of the magnetospheric $r_m$ and corotation radii are shown with the dashed lines. *Bottom four panels:* Radial distribution of of different terms of the Spruit criterion (Eq. 5) in the vicinity of $r_m$ at time $t = 6$ (in the beginning of the unstable regime) for models shown above.

[3] Note that the coefficient $k$ equals to that in Eq. 2.

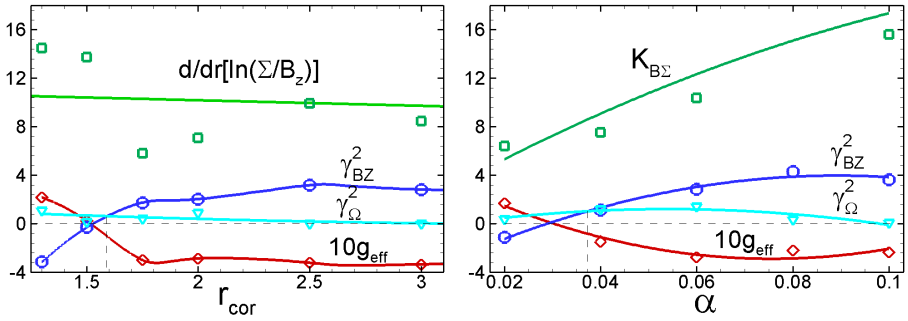



**Figure 8.** *Left Panel:* Dependence of different terms from Spruit's criterion on corotation radius $r_{\rm cor}$. Simulations were performed for stars with $\mu = 1$, $\alpha = 0.02$ and different $r_{\rm cor}$. $g_{\rm eff}$ is multiplied by 10 for clarity. *Right Panel:* Same but for dependence on $\alpha-$ parameter of viscosity. Simulations were done for $\mu = 1$, $r_{\rm cor} = 1.5$ and different $\alpha-$parameters of viscosity.

To check the main hypothesis (which is the dependence of the boundary on the fastness parameter $\omega_s$ and hence the ratio $r_m/r_{\rm cor}$), we measured $r_m$ in each simulation run and marked whether accretion was stable or unstable at a given value of $r_{\rm cor}$ (see Fig. 1).

The accretion rate and $r_m$ generally vary in time. In some cases, accretion is either stable or unstable throughout the entire simulation run, while in other cases it is only marginally stable, and can transition from stable to unstable and back to stable again. In each case, we measured $r_m$ from the simulations using the position of the $\beta_1 = 1$ line for a few moments in time, and marked whether the case was stable or unstable. The $\beta_1 = 1$ line is not a smooth line: it reflects the inner parts of the disc as well as the matter-dominated unstable tongues. We determined $r_m$ using only the inner disc radius and ignoring the tongues. All of these points were used for finding the boundary between stable and unstable regimes of accretion.

### 4.2 Results

Fig. 1 (left panel) shows the results of simulations in the $r_m - r_{\rm cor}$ parameter space for a small misalignment angle of the dipole, $\Theta = 5^\circ$. We can draw an approximate boundary line between stable (red squares) and unstable (blue triangles and green x's) regimes of accretion. This line corresponds to the ratio $r_m/r_{\rm cor} \approx 0.71$, or the fastness parameter $\omega_s \approx 0.6$ (see bold line in the figure). The plot shows that accretion is stable above this line, and is unstable otherwise. In this figure, the values of $r_m$ and $r_{\rm cor}$ are given in radii of the star for user convenience. As expected, instability occurs more easily when $r_m$ is smaller and $r_{\rm cor}$ is larger, that is, when the magnetosphere rotates more slowly than the inner disc and the fastness parameter $\omega_s$ is smaller.

At a sufficiently small ratio of $r_m/r_{\rm cor}$, another transition occurs and matter starts accreting in the *ordered unstable regime*. The boundary between chaotic and ordered unstable regimes approximately corresponds to the condition of $r_m/r_{\rm cor} \approx 0.59$, or fastness parameter $\omega_s \approx 0.45$. This new regime has only been observed in the cases of relatively small magnetospheres, $r_m/R_\star \lesssim 4.2$. At larger magnetospheres, $4.2 \lesssim r_m/R_\star \lesssim 7$, accretion is chaotic (see left panel of Fig. 1).

We should note that at even larger magnetospheres, $r_m \gtrsim 7R_\star$, the RT instability only develops in the external regions of the magnetosphere (e.g., Romanova et al. 2014; Romanova & Owocki 2015) and accretion in two funnel streams dominates. The parameter space with large $r_m$ should be investigated separately

We should also note that when $r_m/r_{\rm cor} > 1$ (or, fastness $\omega_s > 1$), the magnetosphere rotates more rapidly than the inner disc, and the propeller regime is expected. We observed from the simulations that when $r_m \approx r_{\rm cor}$ (fastness parameter $\omega_s = 1$), the magnetosphere pushes the disc outward through the propeller mechanism. The parameter values under which the propeller regime is expected to dominate should be studied separately. In the present study, we draw the $\omega_s = 1$ line as a reminder that the propeller regime is expected near or above this line.

## 5 TWO TYPES OF UNSTABLE REGIME: CHAOTIC AND ORDERED

Here, we describe the two types of unstable regime in greater detail, as observed in the simulations: (1) the *chaotic unstable regime*, where matter accretes in several chaotic, transient tongues, and (2) the *ordered unstable regime*, where one or two tongues form and rotate persistently with the frequency of the inner disc. Below, we discuss these two types of unstable regime for cases of a small tilt of the dipole, $\Theta = 5^\circ$.

### 5.1 Chaotic unstable regime

To demonstrate the chaotic unstable regime, we use the model $\mu 1 c 2.5 \Theta 5 \alpha 0.02$, where the magnetosphere is relatively large ($\mu = 1$) and the corotation radius is $r_{\rm cor} = 2.5$, which corresponds to the period $P_\star \approx 3.9$ in dimensionless units. We observed that matter accretes in several tongues, which form frequently and rapidly disappear. Fig. 2 (left two panels) shows a typical picture of matter flow through the chaotic unstable tongues, which are tall and narrow, and which penetrate the field lines by pushing them aside (right panel).

Fig. 3 shows the temporal evolution of tongues in several consecutive slices of density distribution, separated by the time interval of $\Delta t = 0.5$ [4]. Top two rows show that the

[4] Note that in our units $\Delta t = 1$ corresponds to the period of Keplerian rotation at $r = 1$. However, the inner disc usually rotates with sub-Keplerian velocity, because the disc interacts with the slowly rotating magnetosphere

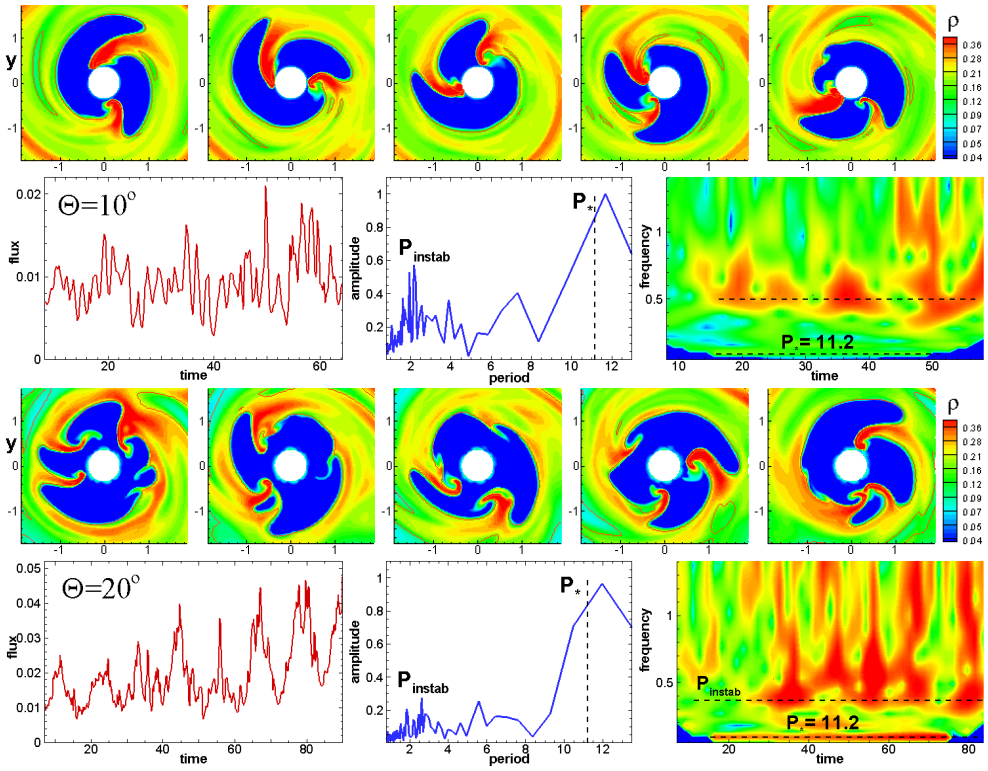



**Figure 9.** *Top two rows:* consecutive xy-slices (times $t = 37 - 39$) and analysis of variability for a larger misalignment angle, $\Theta = 10°$, model $\mu 0.3 c 5 \Theta 10 \alpha 0.02$. *3rd and 4th rows:* same as top two rows, but for $\Theta = 20°$, model $\mu 0.5 c 5 \Theta 20 \alpha 0.02$ (times $t = 30.75 - 32.75$).

tongues are constantly modified, breaking or coalescing on a time-scale of $\Delta t \approx 0.5 - 1$. The $3D-$panels show accretion through chaotic instabilities, with the occasional formation of funnel streams.

The matter from unstable tongues accelerates due to gravity, falls onto the star and releases kinetic energy at the surface of the star, forming hot spots. We use a simple model for the radiation of the spots, suggesting that all kinetic energy of the falling matter is converted into radiation, which is distributed isotropically (see details in Romanova et al. 2004). We calculate the light-curve as seen by a remote observer, located at an angle of $i = 45°$ with respect to the rotational axis of the star (see bottom left panel of Fig. 3). The light-curve shows irregular variations on a time-scale $\approx 1.5$ times shorter than the period of the star, $P_\star = 3.9$. The bottom middle and right panels show the Fourier and wavelet spectra of this light-curve. The wavelet shows different angular frequencies. One of them corresponds to the frequency of the star, $f_\star = 0.26$ (corresponding to the period of $P_\star = 3.9$). Other frequencies are higher, with $f_{\rm inst} \approx 0.3, 0.5$. The Fourier spectrum shows that there are several peaks in the interval of $P_{\rm inst} = 2 - 3.2$, which correspond to the wavelet frequencies. These periods also correspond to the time-scale of variability observed in the light-curve. We suggest that these periods reflect the frequency of formation of the strongest tongues that reach the surface of the star.

Both the wavelet and the Fourier analysis show the presence of the stellar period, which can be associated with the fact that the entire set of unstable temporary spots is oriented around the magnetic pole. The magnetic pole is slightly tilted about the rotational axis (at $\Theta = 5°$ in this case) and the rotation of the star modulates the light from the set of chaotic spots. This is a probable reason for why the stellar period is also observed. Another possible reason is that some matter accretes to the star in funnel streams above the magnetosphere and forms hot spots which tend to rotate with the star. In the present study, we chose an inclination angle of $i = 45°$ because this is where modulation by stellar rotation is expected to be the strongest. If this angle were smaller, then the stellar period would have had a smaller amplitude.

### 5.2 Ordered unstable regime: one- and two-tongue accretion

When the ratio $r_m/r_{\rm cor}$ becomes sufficiently small, unstable accretion becomes ordered: multiple tongues merge, forming one or two ordered tongues. In some cases, two tongues carry a comparable amount of matter flux, while in other cases one of the two tongues may carry more mass. In all cases, the bases of the tongues rotate with the frequency of the inner disc.

Fig. 4 shows a snapshot of unstable accretion in two tongues, model $\mu 0.5 c 3 \Theta 5 \alpha 0.02$. One can see that two ordered matter-dominated tongues push the magnetic field lines apart and penetrate into the deep layers of the magnetosphere, where they transition into regular funnel streams, but very close to the star. The top two panels of Fig. 5 show snapshots of accretion at five consecutive moments in time. The figure shows that initially there was only one tongue, and the second one formed later. One and two-tongue accretion modes are often observed in the same simulation run.

The tongues deposit matter onto the stellar surface and

form one or two hot spots that rotate more rapidly than the star. The light-curve shows regular peaks that reflect the frequency of rotation of these spots (not the frequency of stellar rotation). The Fourier analysis shows a large peak associated with the rotating spots, with a period of $P_{\rm inst} \approx 2-3$. The period of the star, $P_\star = 5.2$, is also visible, but with a smaller amplitude. The wavelet analysis shows frequencies in the range of $f_{\rm inst} \approx 0.3 - 0.6$, which correspond to the peaks observed in the Fourier spectrum.

The main period observed in the light-curve is associated with the rotation of the ordered unstable tongues and approximately corresponds to the period of inner disc rotation. The ordered unstable regime may be an important mechanism in the formation of quasi-periodic oscillations during episodes of enhanced accretion, when the magnetosphere is compressed and the magnetospheric radius can be much smaller than the corotation radius.

### 5.3 The boundary between chaotic and ordered unstable regimes

To find the boundary between the chaotic and ordered unstable regimes, we marked the cases in which one or two unstable tongues carry more mass than the other tongues and labelled these models as green x's in Fig. 1. The approximate position of this boundary corresponds to the ratio $r_m/r_{\rm cor} \approx 0.59$ (the fastness $\omega_s \approx 0.45$ in the cases of relatively small magnetospheres, $r_m/R_\star \lesssim 4.2$. Ordered unstable accretion in one or two tongues dominates below this line. In the cases of larger-sized magnetospheres ($r_m/R_\star \gtrsim 4.2$), only the chaotic unstable regime has been observed.

Simulations show that near the $r_m/r_{\rm cor} \approx 0.59$ line accretion is mainly chaotic, although at some point in a simulation run one or two tongues may start to carry more matter than the other tongues. Accretion may also alternate between ordered and chaotic within the same simulation run. At smaller values of $r_m/r_{\rm cor}$ accretion becomes systematically more ordered, and the frequency associated with the ordered tongues becomes stronger. This means that at smaller values of the $r_m/r_{\rm cor}$ ratio the quality factor $Q = f/\Delta f$ [5] of the quasi-periodic oscillations associated with the ordered unstable tongues is higher. Such an increase in the quality factor is expected during accretion outbursts, when the disc moves inward towards the star.

The diagram in Fig. 6 summarizes the boundaries between the stable and unstable regimes, and between the chaotic and ordered unstable regimes.

## 6 ANALYSIS OF INSTABILITY

In this section, we analyze the dependence of the transition between stable and unstable regimes on different parameters. we are interested in understanding the dependence of accretion mode on the corotation radius $r_{\rm cor}$ and the $\alpha-$parameter of viscosity.

[5] The quality factor is the ratio between the frequency of oscillations and the width of the peak at the half-maximum.

### 6.1 Comparison of stable and unstable cases

To compare the simulation results with the theoretical criterion (Eq. 5), we took two models with the same parameters but different corotation radii: $\mu 2 c 2 \Theta 5 \alpha 0.02$ and $\mu 2 c 3 \Theta 5 \alpha 0.02$, and compared their modes of accretion. In the first model, the corotation radius is $r_{\rm cor} = 2$, and a star is in stable regime of accretion (see left panels of Fig. 7). In the second model, the corotation radius is $r_{\rm cor} = 3$, the star rotates more slowly, and the mode of accretion is unstable. (see right panels of Fig. 7). We then calculated the different terms of the theoretical criterion (Eq. 5) in the vicinity of the magnetospheric radius $r_m$, where the unstable perturbations can occur. To calculate these terms, we took the azimuthally-averaged values of relevant variables and plotted them as a function of radius in Fig. 7. Top panels show that in the stable regime (left panel, $r_{\rm cor} = 2$), $\gamma^2_\Omega > \gamma^2_{B\Sigma}$ at the magnetospheric radius (vertical dashed line), while in the unstable regime (right panel, $r_{\rm cor} = 3$), $\gamma^2_{B\Sigma} > \gamma^2_\Omega$. In both cases, results of the simulations are consistent with the analytical prediction (Eq. 5). Bottom panels show that in the unstable regime the effective gravity is $g_{\rm eff} \approx -0.15$, while in the stable regime it is slightly positive, $g_{\rm eff} \approx 0.06$.

The compression factor $K_{\rm B\Sigma}$ is larger in the unstable regime. Therefore, the term characterizing the instability, $\gamma^2_{B\Sigma}$, is larger in the unstable regime due to both a larger effective gravity term $-g_{\rm eff}$ and a larger compression factor $K_{\rm B\Sigma}$.

### 6.2 Dependence of instability on $r_{\rm cor}$

To better understand the physics of transition between the stable and unstable regimes and its dependence on the $r_{\rm cor}$ parameter, we take the model $\mu 1 c 1.5 \Theta 5 \alpha 0.02$ (which is at the boundary between stable and unstable regimes) and recalculate it at different corotation radii $r_{\rm cor}$ while keeping all the other parameter values fixed ($\mu = 1$, $\Theta = 5^\circ$, $\alpha = 0.02$). We then calculate the main terms from Eq. 5, $\gamma^2_{B\Sigma}$ and $\gamma^2_\Omega$, which determine whether the model is stable or unstable. We also separately calculate the compression factor, $K_{\rm B\Sigma} = \left|\frac{d}{dr} \ln \frac{\Sigma}{B_z}\right|$, and the effective gravity term, $g_{\rm eff}$.

Fig. 8 (left panel) shows that effective gravity $g_{\rm eff}$ decreases with $r_{\rm cor}$, changes sign from positive to negative, and then levels off at some negative value. It levels off because at large corotation radii the angular velocity is small and the centrifugal acceleration term in $g_{\rm eff}$ becomes negligibly small compared with the gravitational acceleration. One can also see that the compression factor $K_{\rm B\Sigma}$ is large, but does vary systematically, and therefore the variation of the instability term $\gamma^2_{B\Sigma}$ is mainly determined by $g_{\rm eff}$. We should note that, although both $g_{\rm eff}$ and the shear term $\gamma^2_\Omega$ are relatively small and do not vary much with $r_{\rm cor}$, $g_{\rm eff}$ becomes important due to its critical sign change during the transition. We conclude that the transition from the stable to the unstable regime is largely due to the variation in effective gravity. The transition occurs at $r_{\rm cor} \approx 1.6$, when $\gamma^2_{B\Sigma} = \gamma^2_\Omega$.

We should note that the point of transition, $r_{\rm cor} \approx 1.6$, is close to the value of $r_{\rm cor} \approx 1.5$, where $g_{\rm eff}$ changes sign from slightly positive to increasingly more negative.

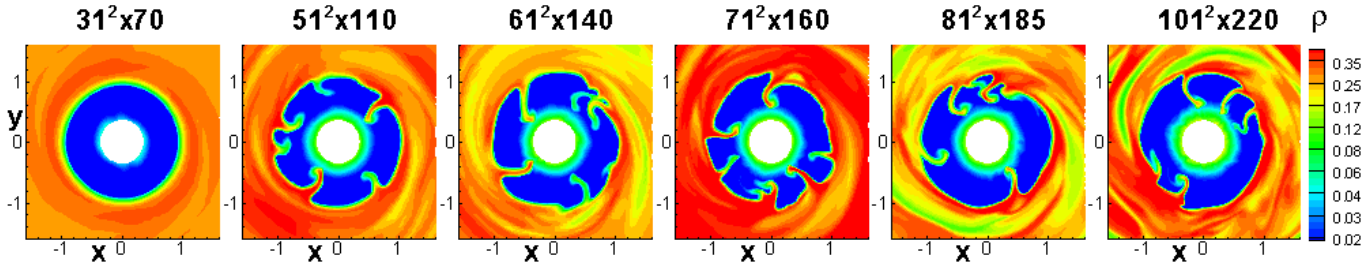



**Figure 10.** A comparison of simulation results for the model $\mu 0.5c1.5\Theta 5\alpha 0.02$ (at time $t = 18$) using different grid resolutions. Simulations show that accretion is stable in the case of the coarsest grid, with $31^2 \times 70$ grids in one of the six sides of the cubed sphere (*left panel*) and is unstable in the cases of the finer grids, $51^2 \times 110$, $61^2 \times 140$, $71^2 \times 160$, $81^2 \times 185$, and $101^2 \times 220$. The color background shows the density distribution in the equatorial plane.

### 6.3 Dependence of instability on $\alpha$

In another set of experiments, we take the same model, $\mu 1c1.5\Theta 5\alpha 0.02$, and vary parameter $\alpha$ in the range of $\alpha = 0.02 - 0.1$. We observed that this initially stable case becomes increasingly more unstable with increasing $\alpha$. We are interested in knowing why this transition happens and why the instability becomes stronger at higher values of $\alpha$.

Fig. 8 (right panel) shows results of our simulations. One can see that at larger $\alpha$, the regime switches from stable to unstable. The transition (where $\gamma^2_{B\Sigma} = \gamma^2_\Omega$) occurs at $\alpha \approx 0.037$. At larger values of $\alpha$, the disc-magnetosphere boundary becomes more unstable due to both the decreasing effective gravity $g_{\rm eff}$ and the increasing compression factor $K_{\rm B\Sigma}$. The shear $\gamma^2_\Omega$ in the disc is relatively small and varies slowly compared with the $\gamma^2_{B\Sigma}$ term, thus having a smaller influence on the transition.

It is interesting to note that the compression factor $K_{\rm B\Sigma}$ increases with $\alpha$. This is probably due to the fact that the radial velocity of matter in the disc increases with $\alpha$: $v_r = \alpha c_s^2/v_K$ (where $c_s$ and $v_K$ are the local sound speed and Keplerian velocity, respectively), and higher gradients of surface density (per unit of magnetic flux) are expected. On the other hand, the overall accretion rate increases with $\alpha$: $\dot{M} \sim v_r \sim \alpha$, which leads to a decrease in the magnetospheric radius: $r_m \sim 1/\dot{M}^{2/7}$, and $g_{\rm eff}$ becomes more negative. The transition between the stable and unstable regimes (where $\gamma^2_{B\Sigma} = \gamma^2_\Omega$) occurs at $\alpha \approx 0.037$, which is near the point $\alpha = 0.028$, where the effective gravity $g_{\rm eff}$ changes the sign. Here, as in the case of varying $r_{\rm cor}$, effective gravity plays an important role in the transition between stable and unstable regimes.

This set of simulations is similar to the simulations performed in our earlier studies, where we investigated the transition between stable and unstable regimes by changing parameter $\alpha$ to vary the accretion rate $\dot{M}$, which we took to be the main factor in determining the mode of accretion (e.g., Kulkarni & Romanova 2008; Romanova et al. 2008). In this paper, our approaches were aimed at a deeper understanding of the physics of transition between the stable and unstable regimes, and its dependence on different parameters.

In realistic discs, the angular momentum transport is probably provided by the magnetic turbulence, supported by the magneto-rotational instability (Balbus & Hawley 1991). The effective $\alpha-$parameter is determined by the ratio of magnetic stress to matter pressure. The $\alpha-$ parameter may be relatively high in the inner parts of the disc, where the magnetic field of the turbulent cells is amplified by the rapid Keplerian rotation of inner disc matter (e.g., Hawley 2000; Armitage 2002). In addition, part of the stellar magnetic flux penetrates into the disc and increases the magnetic stress in the inner disc, so that the $\alpha-$parameter can be as high as $\alpha = 0.3 - 1$ (Romanova et al. 2011, 2012; Lii et al. 2014). This is why we also performed test simulation runs at a relatively high parameter of viscosity, $\alpha = 0.1$. These simulations have shown that instability is stronger when $\alpha = 0.1$ than in the cases of $\alpha = 0.02$, and that the boundary between stable and unstable regimes is expected to be higher, closer to the $r_m/r_{\rm cor} \approx 1$ line, though additional research is required to find this line.

## 7 DEPENDENCE OF INSTABILITY ON GRID RESOLUTION

To investigate the dependence of instability on grid resolution, we chose a model with such parameters as make it close to the boundary between stable and unstable regimes of accretion: $\mu 0.5c1.5\Theta 5\alpha 0.02$. First, we ran simulations of this model using two grid resolutions, $31^2 \times 70$ and $61^2 \times 140$. We noticed that the $31^2 \times 70$ case is stable, while the $61^2 \times 140$ case is unstable. We then performed a set of simulations of this model at several other grid resolutions: $51^2 \times 110$, $71^2 \times 160$, $81^2 \times 185$, and $101^2 \times 220$. We observed that instability is present at all finer grid resolutions, including $51^2 \times 110$ and finer (see Fig. 10). We compared matter fluxes at all grid resolutions, and found that while matter flux values are substantially different when comparing the $31^2 \times 70$ and the $61^2 \times 140$ cases, there is smaller difference in the matter flux values of all the finer grid resolutions: $51^2 \times 110$, $61^2 \times 140$, $71^2 \times 160$, $81^2 \times 185$, and $101^2 \times 220$ (see Fig. 11). These comparisons show that at a coarse grid resolution, numerical viscosity suppresses the development of the RT instability, while at sufficiently fine grid resolutions, the results do not depend much on grid resolution. Numerical viscosity probably plays the same role as regular viscosity in suppressing the smallest-scale perturbation modes, as discussed by Chandrasekhar (1961).

## 8 DEPENDENCE OF INSTABILITY ON $\Theta$

The above simulations were performed for a small tilt of the dipole magnetosphere, $\Theta = 5^\circ$. It is important to know

whether accretion through RT instability is present in the cases of larger tilts. To answer this question, we performed a series of simulation runs for a larger tilt, $\Theta = 20^\circ$, with the same goal in mind: to find the boundary between stable and unstable regimes of accretion. Fig. 1 (right panel) shows the results of simulations. We observed that accretion becomes unstable in many instances, and the boundary between stable and unstable regimes corresponds to the ratio $r_m/r_{\rm cor} \approx 0.67$ (fastness parameter $\omega_s \approx 0.54$). This line is very close to the boundary line obtained for $\Theta = 5^\circ$ (see dash-dot-dotted line right above the bold line in the right panel of Fig. 1). This result is in agreement with our hypothesis that $g_{\rm eff}$ is the main factor in determining the strength of the instability.

To better understand the unstable accretion onto stars with different tilts of the dipole field, we performed test simulation runs at different tilts of the dipole: $\Theta = 10^\circ, 15^\circ, 20^\circ, 30^\circ, 40^\circ$ and $60^\circ$. We focused on the ordered unstable regime and therefore used relatively small magnetospheres, $\mu = 0.3 - 0.5$ and large values of $r_{\rm cor}$. One of the questions was whether this type of unstable accretion will take place in the cases of larger tilts of the dipole. First, we performed simulation runs for relatively small tilts, $\Theta = 10^\circ, 15^\circ, 20^\circ, 30^\circ$. Fig. 9 shows $xy-$slices for two of these angles, $\Theta = 10^\circ$ and $20^\circ$. The xy-slices of density distribution show ordered unstable accretion in one or two tongues in the case of the smallest tilt, $\Theta = 10^\circ$ (top row of xy-slices). However, at a larger tilt, $\Theta = 20^\circ$, accretion becomes more chaotic (bottom row of xy-slices).

We also performed frequency analyses of the light-curves, which were calculated from the moving hot spots on the stellar surface, as seen at an inclination angle of $i = 45^\circ$. The light-curve for the $\Theta = 10^\circ$ case (see second row in Fig. 9) shows that the main source of variability is the rotation of unstable ordered spots. However, modulation by stellar rotation is also observed. The Fourier spectrum shows a peak with a period of $P_{\rm inst} \approx 2$, associated with the instability, and a peak associated with the period of the star, $P_\star \approx 11.2$. The wavelet spectrum mainly shows the frequency $f_{\rm inst} \approx 0.5$, associated with the instability.

In the case of $\Theta = 20^\circ$ the amplitude of the oscillations associated with instability is smaller, and the light-curve is mainly determined by the rotation of the star, while the instabilities provide a high-frequency modulation of the main light-curve. The presence of instability is weak in the Fourier spectrum of the $\Theta = 20^\circ$ case, but clearly visible in the wavelet spectrum (see bottom row of Fig. 9).

In the cases of even larger tilts of the dipole, $\Theta = 30^\circ$, $\Theta = 40^\circ$ and $60^\circ$, the light-curve is still modulated by the unstable component of accretion, but the amplitude of the modulation is smaller than in the case of $20^\circ$.

## 9 COMPARISON BETWEEN RELATIVISTIC AND NON-RELATIVISTIC CASES

The results of current simulations are relevant for non-relativistic stars. However, in case of neutron stars, we should take into account the relativistic gravitational potential, which provides a deeper gravitational well and may enhance instability, in particular when the unstable tongues move closer to the star. A relativistic potential has been used

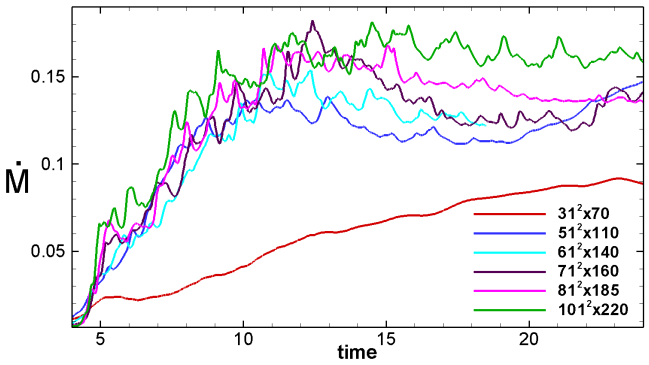



**Figure 11.** Matter fluxes $\dot{M}$ onto the star as a function of time for model $\mu 0.5 c1.5 \Theta 5 \alpha 0.02$, obtained at 6 different grid resolutions.

in most of our prior simulations (Kulkarni & Romanova 2008, 2009; Romanova et al. 2008; Bachetti et al. 2010).

In this paper, we consider non-relativistic stars to be sure that the instability mechanism is present even in the cases of shallower, non-relativistic potential wells. However, in application to neutron stars it is important to take into account the relativistic effects and to compare the differences between instabilities in non-relativistic and relativistic cases. It would be too time-consuming to recalculate all the cases for relativistic stars. Instead, we chose one representative model, $\mu 1 c3 \Theta 5 \alpha 0.02$, and recalculated it taking into account the relativistic corrections. To model the relativistic effects we chose the Paczyński-Wiita (PW) pseudo-relativistic potential (Paczyński & Wiita 1980), $\Phi(r) = GM_\star/(r - r_g)$, where $r_g = 2GM\star/c^2$ is the gravitational (Schwarzschild) radius. For a typical neutron star with mass $M_\star = 1.4 M_\odot$ and radius $R_\star = 10$ km, the ratio $r_g/R_\star = 0.145$.

We found the results to be similar: instability of comparable strength has developed, with two ordered tongues forming and rotating with the frequency of the inner disc. Fig.12 shows xy-slices of these two models for the same moment in time. The matter flux onto the star (bottom panel) is about 20% higher in the relativistic case. However, this does not affect the instability pattern qualitatively. We should note that the PW potential gives a steeper gravitational well than the fully relativistic approach, and therefore the relativistic effects will be even weaker in a more realistic relativistic case.

We conclude that the main effect of enhanced gravity is enhanced accretion rate to the star, $\dot{M}$. However, the difference in accretion rate between the non-relativistic and the PW pseudo-relativistic cases is $\sim 20\%$, which leads to a factor of only $1.2^{1/7} \approx 1.03$ difference in the magnetospheric radius $r_m$. This difference is small, which is why relativistic effects do not enhance instability significantly.

## 10 APPLICATION TO DIFFERENT MAGNETIZED STARS

The results of our simulations can be applied to different types of magnetized stars.

### 10.1 Application to CTTSs

Classical T Tauri stars stars show variability on different timescales, ranging from hours to months (Herbst et al. 1994).

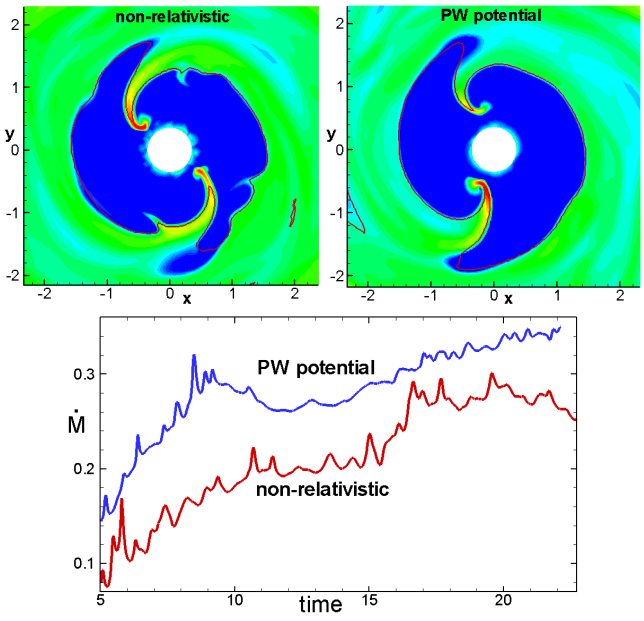



**Figure 12.** *Top panels:* density distribution of matter in the equatorial (xy) slice in the model with $\mu = 1$, $r_{\rm cor} = 3$ (model $\mu 1 c 3 \Theta 5 \alpha 0.02$) at time $t = 20$ in non-relativistic (left) and relativistic (right) cases. *Bottom panel:* Matter fluxes to the star in non-relativistic and relativistic cases.

In most cases, the causes of variability have not been understood.

Recent observations of the light-curves from young stars in the NCG 2264 cluster, obtained with the *CoRoT* telescope, show that many stars have irregular variability (Alencar et al. 2010). One of the important time-scales corresponds to that expected in the unstable regime of accretion, that is, a few peaks per rotational period of the inner disc (Stauffer et al. 2014; Cody et al. 2014).

The ordered unstable regime may also be important during the periods of accretion outbursts, observed in EXor and FU Ori-type stars (e.g., Audard et al. 2014). In these stars, the accretion rate is greatly enhanced, the magnetosphere is compressed, and the magnetospheric radius may be much smaller than the corotation radius. Therefore, conditions become favorable for ordered unstable accretion in one or two ordered tongues. Recently, a very short period (of $\sim 1$ day) was discovered in the protostar V1647 Ori during its two recent accretion outbursts (Hamaguchi et al. 2012). Hamaguchi et al. (2012) suggested that the puzzling short-term X-ray variability of V1647 Ori was probably due to the rotational modulation of the hot spots on the stellar surface. However, as the authors noted, the $\sim 1$ day period corresponds to rotation at near-breakup speed of V1647 Ori. We suggest that it is improbable that a star rotates so rapidly. Instead, the rapidly-rotating regions of enhanced plasma found in the empirical model of Hamaguchi et al. (2012) may be connected with the rotation of the ordered unstable tongues in the ordered unstable regime of accretion, which is highly likely to occur during accretion outbursts.

### 10.2 Application to accreting white dwarfs

A few types of accreting white dwarfs have strong magnetic fields. In the Intermediate Polars (hereafter IPs), the magnetosphere disrupts the disc at $r_m \gtrsim 10 R_\star$, which is larger than the radii considered in this paper. Simulations of accretion to large magnetospheres (Romanova et al. 2014) show that matter of the inner disc only partially penetrates the magnetosphere, and most of the matter flows onto the star in two funnel streams (above the magnetosphere), forming two ordered hot spots on the surface of the star. In these stars, the light-curves reflect the period of stellar rotation, and are expected to be periodic. This process may explain the periodic light-curves of IPs.

There is another class of accreting white dwarfs, called Dwarf Novae (DNs), that do not show period, but rather quasi-periodic oscillations are observed during accretion outbursts (Warner et al. 2004). The highest-frequency oscillations (called Dwarf Novae Oscillations, or DNOs) have typical time-scales of tens of seconds. The nature of these oscillations has not yet been understood. It is possible that DNs are weakly magnetized white dwarfs whose magnetospheres are strongly compressed during accretion outbursts, with $r_{\rm cor} >> r_m$. This condition is favorable for ordered unstable accretion, where one or two ordered tongues are the cause of quasi-periodic variability. Variation in accretion rate leads to variation in the position of the inner disc and frequency of the tongues, which may possibly explain the nature of DNOs.

### 10.3 Application to accreting neutron stars

The model can also be applied to accreting X-ray millisecond pulsars (AMXPs), where matter of the inner disk accretes onto a weakly magnetized ($B \sim 10^8 - 10^9$G) neutron star during accretion outbursts (van der Klis 2006; Ibragimov & Poutanen 2009; Patruno & Watts 2012). Observations show pulsations associated with the rotation of the star, and also one or two peaks associated with the high-frequency quasi-periodic oscillations. The frequencies of QPOs vary in time from values that are lower than the frequency of the star to values that are much higher than the frequency of the star. The origin of these QPOs is still not well understood. We suggest that, in AMXPs, one of the QPO frequencies may be associated with the rotation of unstable tongues in the unstable regime of accretion which onset when the accretion rate increases and the magnetospheric radius approaches the value $r_m \approx 0.7 r_{\rm cor}$. The chaotic tongues rotate with the frequency of the inner disk, reflecting the QPO frequency (see also Bachetti et al. 2010). At even higher accretion rates, the disk moves even closer to the star and, at $r_m \lesssim 0.6 r_{\rm cor}$, the ordered unstable regime dominates. The quality factor, Q, increases due the increasing dominance of the ordered unstable regime. This is consistent with the observations, which show that the frequencies of QPOs increase with X-ray flux (which is usually proportional to the accretion rate) (e.g., Papitto et al. 2007), and the quality factor increases with increasing QPO frequency (e.g., van der Klis 2006; Barret et al. 2007).

We expect that the transition from the stable to the unstable regime should lead to a decrease of the pulsed fraction in the observed radiation (e.g., Kulkarni & Romanova 2008). The pulsations are associated with stable (two funnel stream)

magnetospheric accretion, where two hot spots form and rotate with the frequency of the star. In contrast, in the unstable regime, most of the matter flows in irregular tongues, and the expected fraction of pulsed radiation is smaller. Interestingly, a drop in the pulse fraction has been recently observed in the AMXP SAX J1808.4-3658 (Bult & van der Klis 2015). The pulse fraction decreased dramatically when the QPO frequency (associated with the frequency of the inner disk) increased and became comparable to the stellar frequency. The drop in the pulse fraction may be connected with the transition from stable to unstable accretion. However, these observations show that the transition occurs when $r_m \approx r_{\rm cor}$. This is different from the $r_m = 0.7 r_{\rm cor}$ boundary found in our simulations at a small parameter of viscosity ($\alpha = 0.02$). Simulations show that at larger values of $\alpha$ (e.g., $\alpha = 0.1$) the boundary corresponds to larger values of $r_m/r_{\rm cor}$. Our model can explain the transition of the pulse fraction at high $\alpha-$parameters of viscosity.

## 11 CONCLUSIONS

A new set of simulations has been performed with the goal of investigating the boundary between stable and unstable regimes of accretion and the properties of unstable accretion. Simulations were performed at twice as high a grid resolution as in our earlier studies (Kulkarni & Romanova 2008, 2009; Romanova et al. 2008). A low viscosity parameter in the disc ($\alpha = 0.02$) was used in most of the simulation runs. The main results of the new investigations are the following:

**1.** We found that the boundary between stable and unstable regimes of accretion depends almost entirely on the fastness parameter $\omega_s$ (or the ratio between the magnetospheric radius and the corotation radius, $r_m/r_{\rm cor}$). Accretion is unstable if $\omega_s \lesssim 0.6$ ($r_m/r_{\rm cor}) \lesssim 0.71$), and is stable otherwise. The main simulations were performed at a small misalignment angle of the dipole, $\Theta = 5^\circ$, and low viscosity in the disc, $\alpha = 0.02$.

**2.** Below the $\omega_s \approx 0.6$ ($r_m/r_{\rm cor} \approx 0.71$) line, accretion proceeds in the *chaotic unstable regime* through several unstable tongues. The light-curve from the hot spots looks chaotic, and the spectral analysis shows several frequencies associated with the chaotic tongues. One of the frequencies often corresponds to the frequency of the inner disc, because the set of short-lived tongues rotates with the angular frequency of the inner disc. The frequency of the star is usually present in the frequency spectra if the simulation runs are sufficiently long.

**3.** A new type of unstable regime of accretion, the *ordered unstable regime*, was found in the cases of slowly rotating stars, $\omega_s \lesssim 0.45$ ($r_m/r_{\rm cor} \lesssim 0.59$). In this regime, matter accretes in one or two ordered unstable tongues that rotate with the frequency of the inner disc. The ordered unstable regime has been observed in the cases of relatively small magnetospheres, $r_m/R_\star \lesssim 4.2$.

**4.** In the cases of larger misalignment angles of the dipole, accretion through instabilities is also present. The boundary between stable and unstable regimes was found for the case of $\Theta = 20^\circ$. This boundary, $\omega_s = 0.55$, is very close to the one obtained in the case of a small tilt, $\Theta = 5^\circ$, because in both cases the instability is mainly determined by the effective gravity. However, in cases of increasingly larger tilts, more matter flows above the magnetosphere in regular funnel streams and forms two hot spots near the magnetic poles, determining the regular sinusoidal light-curve that represents the period of the star. The matter accreting though instabilities provides the high-frequency modulation of the main light-curve. The amplitude of the oscillations decreases with $\Theta$ because a strongly tilted dipole breaks the unstable tongues.

**5.** At a *higher viscosity* in the disc, $\alpha = 0.1$, chaotic instability becomes more irregular, and variability on different time-scales is observed in the light-curve. The frequency associated with the inner disc rotation is seen in both the Fourier and the wavelet spectra, while the frequency of the star has a much lower amplitude.

**6.** Analysis *of the causes* of instability in the borderline cases between stable and unstable regimes shows that: (a) Increasing the *corotation radius* $r_{\rm cor}$ (while fixing all other parameters) leads to the larger negative values of effective gravity $g_{\rm eff}$ causing the transition from the stable to the unstable regime of accretion. We believe the sign change of $g_{\rm eff}$ to be the main factor in this transition. (b) Increasing the *viscosity parameter* $\alpha$ leads to a higher compression factor $K_{\rm B\Sigma}$ which leads to stronger instability.

**7.** A grid convergence has been observed at high grid resolutions. Simulations show that instabilities are only suppressed at the coarsest grid ($31^2$ angular cells in each block), while at all finer grids ($51^2$ and finer) accretion through instabilities is present, and is similar in all cases.

**8.** A comparison of relativistic and non-relativistic cases shows that instability is somewhat stronger in the relativistic cases. However, the relativistic potential is not the main factor in determining the mode of accretion.

**9.** All of the above results were obtained for magnetospheres with $r_m/R_\star \lesssim 7$ and should not be generalized to stars with large magnetospheres. Separate studies show that in the cases of large magnetospheres, instabilities are only present in the external parts of the magnetosphere, while matter accretes to the star in two ordered funnel streams (Romanova et al. 2014).

**10.** The results can be applied to different types of accreting magnetized stars. The main findings are the following:

(a) Accretion in ordered unstable tongues can be important during accretion outbursts, when the inner disc moves inward, compressing the magnetosphere, and the ratio $r_m/r_{\rm cor}$ is small. The frequency of the rotating tongues corresponds to the frequency of the inner disc and may be seen as a QPO feature in the frequency spectra. The QPO frequency increases when the inner disc moves inward. The quality factor also increases during the inward motion of the disc.

(b) When a star is observed for a few periods of stellar rotation, as in CTTSs, the frequency of the oscillations associated with the ordered unstable tongues may be mistaken for the frequency of the star.

(c) A star may alternate between stable and unstable regimes of accretion, thus showing an intermittency in its pulsations.

**Acknowledgments**

Authors thank Alexander Koldoba for an earlier-developed 'cubed sphere' code and the referee for critical reading of the paper. Resources supporting this work were provided by the NASA High-End Computing (HEC) Program through the NASA Advanced Supercomputing (NAS) Division at Ames Re-

search Center and the NASA Center for Computational Sciences (NCCS) at Goddard Space Flight Center. The research was supported by NASA grant NNX14AP30G and NSF grant AST-1211318.

## APPENDIX A: MAGNETOSPHERIC RADIUS

It is important to know the relationship between the magnetospheric radii obtained from the balance of stresses, $\beta_1 = 1$ (which have been obtained from our 3D MHD numerical simulations and used in our paper), and the magnetospheric radii derived from the theoretical formula, 2, which is widely used for estimating $r_m$ (in the cases where the values of $\mu_\star$, $\dot{M}$ and $M_\star$ are known). In our simulations, we can compare these two radii by (1) taking one of them from the condition $\beta_1 = 1$, and (2) taking the second one from Eq. 2, using parameters $\mu_\star$, $M_\star$ and $\dot{M}$, whose values are known from our simulations. Comparisons of these radii will help us derive the unknown coefficient $k$, as well as check the overall dependencies in Eq. 2.

For these comparisons, we first convert the theoretically-derived magnetospheric radius (Eq. 2) to the dimensionless form (see procedure of dimensionalization in Sec. 3.4 and resulting Eq. 6) [6]. We re-write Eq. 6 in a more general form:

$$r_m = k(\mu^2/\dot{M})^n \ , \tag{A1}$$

and search for coefficients $k$ and powers $n$. All variables are dimensionless, but we removed the tilde's for convenience. Note that coefficient $k$ is exactly the same as in Eq. 2, and the power $n$ can be different from $n = 2/7$ used in the theoretical formula.

Next, we take our models with different values of parameters $\mu$ and $r_{\rm cor}$, and find $r_m$ from the condition $\beta_1 = 1$. We also measure the dimensionless matter flux $\dot{M}$ and calculate the value $\mu^2/\dot{M}$. We then plot $r_m$ versus $\mu^2/\dot{M}$. $\mu$ is a parameter of the model, and is fixed in each model. However, the accretion rate $\dot{M}$ varies in time. In some cases, the accretion rate levels off at a constant value, in spite of the regime being strongly unstable, as shown in the left panel of Fig. A1. Alternatively, it may vary strongly (by a factor of 2-3), as in the cases of the chaotic unstable regime. This is why the main dispersion of points is expected to arise from the variation of $\dot{M}$. We often took several different points in time within the same simulation run to see how the variation in accretion rate would affect the resulting radius [7].

To measure the magnetospheric radius, we used the condition $\beta_1 = 1$. However, in the unstable regime, the magnetospheric radius often has a complex shape, and the $\beta_1 = 1$ line is not truly circular. To obtain $r_m$ we approximate the inner boundary using the procedure shown in Fig. A1, where the circle approximately reflects the inner boundary. We should note that, in any particular simulation run, the value of $r_m$ does not vary much, which may be the result of a weak (expected) dependence on the accretion rate: $r_m \sim \dot{M}^{-2/7}$. For example, variation of $\dot{M}$ by a factor of 3 leads to the variation of $r_m$ by a factor of 1.3.

Figure A2 shows the results of simulation runs in the stable and unstable regimes (left and right panels, respectively). One can see that in both cases the magnetospheric radius increases with parameter $\mu^2/\dot{M}$, and the best-fit curve is a power-law (see dashed lines), with the power of $n = 0.22$ in the unstable regime and $n = 0.19$ in the stable regime. The plot also helped derive coefficient $k$, which is $k \approx 0.78$ in the stable regime and $k \approx 0.89$ in the unstable regime. Therefore, we expect the formula for the magnetospheric radius to be in the following form:

$$r_m{}^{\rm stable} \approx 0.78\big[\mu_\star^4/(\dot{M}^2 G M_\star)\big]^{0.095} \ , \tag{A2}$$

$$r_m{}^{\rm unstable} \approx 0.89\big[\mu_\star^4/(\dot{M}^2 G M_\star)\big]^{0.11} \ . \tag{A3}$$

In both formulae, the power $n$ is smaller than the power $1/7 \approx 0.146$ in theoretical formula 2. This issue has been analyzed in detail by Kulkarni & Romanova (2013)[8], who concluded that the power $n$ is smaller than in the theoretical formula due to the compression of the magnetosphere by the disc and the non-dipole shape of the external regions of the magnetosphere. This may also be the reason for why in the stable regime the power $n$ is smaller than in the unstable regime: in the unstable regime, the compression is expected to be smaller due to the penetration of matter in unstable tongues.

We can estimate the difference between using the theoretical formula 2 and formulae A2 or A3. For comparisons, we take Eq. A1 in the form for stable regime, $r_m = 0.78(\mu^2/\dot{M})^{0.19}$ and in the form corresponding to Eq. 2, $r_m = k(\mu^2/\dot{M})^{2/7}$ and find $k = 0.78(\mu^2/\dot{M})^{-0.095}$. Then we note, that in our model, $r_m/R_\star$ varies in the range of $2-6$ which corresponds to $0.2 \lesssim \mu^2/\dot{M} \lesssim 80$. For this range, we obtain $0.50 \lesssim k \lesssim 0.90$. Similarly, for the unstable regime we find $k = 0.89(\mu^2/\dot{M})^{-0.026}$ and condition $0.80 \lesssim k \lesssim 0.93$. One can see that in the case of small magnetospheres $2 \lesssim r_m/R_\star \lesssim 6$, theoretical formula 2 can be used to describe the stable regime, if $0.50 \lesssim k \lesssim 0.90$, and the unstable regime, if $0.80 \lesssim k \lesssim 0.93$.

## APPENDIX B: REFERENCE VALUES IN THE TABLE

Table B shows sample values of physical parameters for different types of stars. See Sec. 3 for a detailed description.

## REFERENCES

Alencar, S. H. P. et al., 2010, A&A, 519, A88
Altamirano D., Casella P., Patruno A., Wijnands R., van der Klis M., 2008, ApJ, 674, L45
Armitage, P. 2002, ApJ, 330, 895

[6] Here, we suggest that the mass of the star is fixed at $M_\star = M_0$ so that the dimensionless mass $\widetilde{M}_\star = 1$. We also consider only the cases with $\alpha = 0.02$.

[7] $r_m$ varies in time, because stresses vary in time. Note that finding $r_m$ does not require stationarity.

[8] Kulkarni & Romanova (2013) performed similar comparisons of radii for 3D models in stable regime, where the magnetic dipole is tilted by somewhat larger angle, $\Theta = 15^\circ$ and obtained the dependence $r_m \sim (\mu^2/\dot{M})^{0.2}$ . Our dependence for stable regime is very close to one derived by these authors.

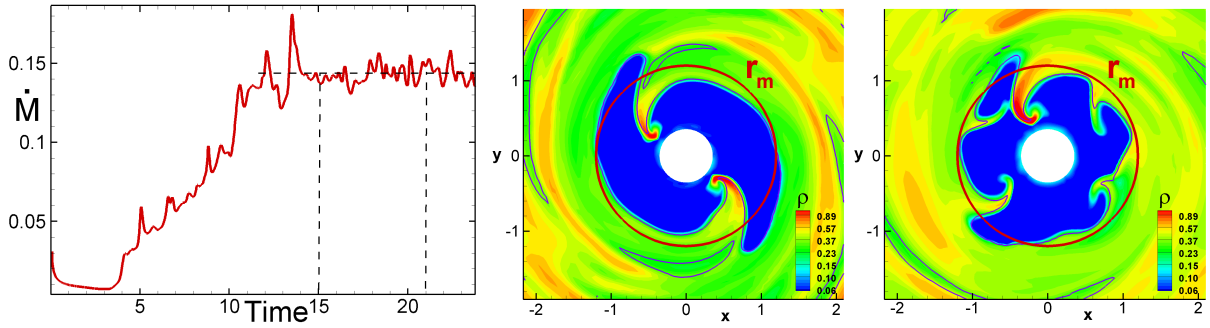



**Figure A1.** *Left panel:* Temporal variation of the dimensionless matter flux $\dot{M}$ in one of models in the unstable regime, $\mu 0.5 c 2.5 \Theta 5 \alpha 0.02$. *Middle and right panels* show the equatorial slices of the density distribution at time $t = 15$ and $t = 21$. The thin purple line corresponds to condition $\beta_1 = 1$ (see Eq. 1). Thick solid line shows the approximate position of the magnetopsheric radius.

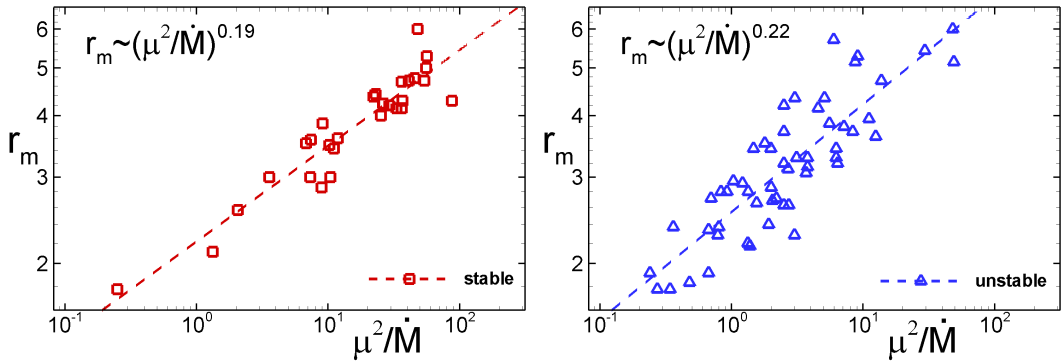



**Figure A2.** *Left panel:* The magnetospheric radii taken from simulations in the stable regime, $r_m$ (measured in stellar radius $R_\star$) versus the value $\mu^2/\dot{M}$. *Right panel:* same, but for the unstable regime. Dashed lines represent the best power fit.

| | CTTSs | White dwarfs | Neutron stars |
|---|---|---|---|
| $M_\star(M_\odot)$ | 0.8 | 1 | 1.4 |
| $R_\star$ | $2R_\odot$ | 5000 km | 10 km |
| $B_\star$ (G) | $10^3$ | $10^6$ | $3 \times 10^8$ |
| $R_0$ (cm) | $4 \times 10^{11}$ | $1.4 \times 10^9$ | $2.9 \times 10^6$ |
| $v_0$ (cm s$^{-1}$) | $1.6 \times 10^7$ | $3 \times 10^8$ | $8.1 \times 10^9$ |
| $\rho_0$ (g cm$^{-3}$) | $2.8 \times 10^{-11}$ | $7.9 \times 10^{-8}$ | $1.0 \times 10^{-5}$ |
| $\Sigma_0$ (g cm$^{-2}$) | 11.0 | 112.5 | 28.9 |
| $\Omega_0$ (s$^{-1}$) | $4 \times 10^{-5}$ | 0.21 | $2.8 \times 10^3$ |
| $f_0$ | 0.55 day$^{-1}$ | $3.2 \times 10^{-2}$ Hz | $4.5 \times 10^2$ Hz |
| $P_0$ | 1.8 days | 29 s | 2.2 ms |
| $\mu_\star$ (Gcm$^3$) | $2.7 \times 10^{36}$ | $1.2 \times 10^{32}$ | $1.0 \times 10^{27}$ |
| $\dot{M}_0$ ($M_\odot$yr$^{-1}$) | $2.8 \times 10^{-7}$ | $1.9 \times 10^{-7}$ | $6.5 \times 10^{-8}$ |

**Table B1.** Sample values of physical parameters for different types of stars. See Sec. 3 for a detailed description.


Arons, J. & Lea, S.M. 1976, ApJ, 207, 914

Audard, M., Ábrahám, P., Dunham, M. M., Green, J.D., Grosso, N. et al. 2014, Accepted for publication as a review chapter in Protostars and Planets VI, University of Arizona Press (2014), eds. H. Beuther, R. Klessen, C. Dullemond, Th. Henning

Bachetti, M., Romanova, M. M., Kulkarni, A., Burderi, L., di Salvo, T. 2010, MNRAS, 403, 1193

Balbus, S.A. & Hawley, J. F. 1991, ApJ, 376, 214

Barret, D., Olive, J,-F,, Miller, M. C. 2007, MNRAS, 376, 1139

Bessolaz N., Zanni C., Ferreira J., Keppens R., Bouvier J. 2008, A&A, 478, 155

Bouvier J., Alencar S. H. P., Harries T. J., Johns-Krull C. M., Romanova M. M., *Protostars and Planets V*, Eds. Reipurth B., Jewitt D., Keil K. (University of Arizona Press, Tucson, 2007) 479

Bult, P., van der Klis, M. 2015, ApJ, 798, L29

Campbell, C.G. 1992, Geophys. Astrophys. Fluid Dynamics, 63, 179

Chandrasekhar, S., 1961, *Hydrodynamic and Hydromagnetic Stability*. Clarendon, Oxford, p. 466

Cody A. M., Stauffer, J., Baglin, A., Micela, G., Rebull, L. M., Flaccomio, E., Morales-Caldern, M. et al., 2014, AJ, 147, 47 pp

Donati, J.-F., Jardine, M. M., Gregory, S. G., et al., 2007, MNRAS 380, 1297

Ghosh, P., 2007, Rotation and Accretion Powered Pulsars: World Scientific Series in Astronomy and Astrophysics – Vol. 10. Edited by Pranab Ghosh. Published by World Scientific Publishing Co., Pte. Ltd., Singapore

Ghosh, P., Lamb, F. K., 1978, ApJ, 223, L83

Hamaguchi, K., Grosso, N., Kastner, J. H., Weintraub, D. A., Richmond, M. et al. 2012, ApJ, 754, 9pp

Hawley, J. F. 2000, ApJ, 528, 462

Hellier, C. 2001, Cataclysmic variable stars, (Springer, Berlin 2001)

Herbst, W., Herbst, D. K., Grossman, E. J., Weinstein, D. 1994, AJ, 108, 1906

Ibragimov, A. & Poutanen, J., MNRAS, 400, 429

Illarionov, A. F., & Sunyaev, R. A. 1975, A&A, 39, 185
Johns-Krull C. M., 2007, ApJ, 664, 975
Kaisig, M., Tajima, T., & Lovelace, R. V. E. 1992, ApJ., 386, 83
Koldoba, A. V., Romanova, M. M., Ustyugova, G. V., Lovelace, R. V. E. 2002, ApJ, 576, L53
Koldoba, A. V., Ustyugova, G. V., Romanova, M. M., Lovelace, R. V. E. 2008, MNRAS, 388, 357
Kulkarni, A. K., & Romanova, M. M., 2005, ApJ, 633, 349
Kulkarni, A., & Romanova, M.M. 2008, ApJ, 386, 673
Kulkarni, A., & Romanova, M.M. 2009, ApJ, 398, 1105
Kulkarni, A., & Romanova, M.M. 2013, MNRAS, 433, 3048
Kurosawa R. and Romanova M. M., MNRAS 2013, 431, 2673
Lamb, F. K., Pethick, C. J., Pines, D. 1973, ApJ, 184, 271
Lii, P.S., Romanova, M.M., Ustyugova, G.V., Koldoba, A.V., Lovelace, R.V.E. 2014, MNRAS, 441, 86
Long, M., Romanova, M.M., & Lovelace, R.V.E. 2005, ApJ, 634, 1214
Long, M., Romanova, M.M., & Lovelace, R.V.E. 2007, MNRAS, 374, 436
Long, M., Romanova, M.M., & Lovelace, R.V.E. 2008, MNRAS, 386, 1274
Lovelace, R.V.E., Romanova, M.M., Bisnovatyi-Kogan, G.S. 1999, ApJ, 514, 368
Lovelace, R.V.E., Romanova, M.M., Bisnovatyi-Kogan, G.S. 1995, MNRAS, 275, 244
Lubow, S.H., & Spruit, H.C. 1995, ApJ, 445, 337
Orlando, S., Sacco, G. G., Argiroffi, C., Reale, F., Peres, G., Maggio, A. 2010, A&A, 510, 12pp
Paczyński B. & Wiita P. J. 1980, A&A, 88, 23
Papitto, A., di Salvo, T., Burderi, L., Menna, M. T., Lavagetto, G., Riggio, A. 2007, MNRAS, 375, 971
Review to appear in "Timing neutron stars: pulsations, oscillations and explosions", T. Belloni, M. Mendez, C.M. Zhang Eds., ASSL, Springer; arxiv1206.2727
Powell, K.G., Roe, P.L., Linde, T.J., Gombosi, T.I., & De Zeeuw, D.L. 1999, J. Comp. Phys., 154, 284
Pringle, J.E., & Rees, M.J. 1972, A&A, 21, 1
Rastätter, L. & Schindler, K. 1999, ApJ, 524, 361
Romanova, M.M. & Kulkarni, A.K. 2009, MNRAS, 398, 701
Romanova, M.M., Kulkarni, A.K., Lovelace, R.V.E. 2008, ApJ Letters, 273, L171
Romanova, M. M., Ustyugova, G. V., Koldoba, A. V., Lovelace, R.V.E., 2002, ApJ, 578, 420
Romanova, M. M., Ustyugova, G. V., Koldoba, A. V., Wick, J. V., Lovelace, R. V. E., 2003, ApJ, 595, 1009
Romanova, M. M., Ustyugova, G. V., Koldoba, A. V., Lovelace, R. V. E., 2004, ApJ, 610, 920
Romanova, M.M., Ustyugova, G.V., Koldoba, A.V., Lovelace, R.V.E. 2011, MNRAS, 416, 416
Romanova, M.M., Ustyugova, G.V., Koldoba, A.V., Lovelace, R.V.E. 2012, MNRAS, 421, 63
Romanova, M.M., Lovelave, R.V.E., Bachetti, M., Blinova, A.A., Koldoba, A.V., et al. 2014, Physics at the Magnetospheric Boundary, Geneva, Switzerland, Edited by E. Bozzo; P. Kretschmar; M. Audard; M. Falanga; C. Ferrigno; EPJ Web of Conferences, Volume 64
Romanova, M.M., & Owocki, S.P. 2015, Space Science Reviews, 191, 339
Rucinski S. M. et al., 2008, MNRAS, 391, 1913
Shakura, N.I., & Sunyaev, R.A. 1973, A&A, 24, 337
Stauffer, J., Cody, A.M., Baglin, A., Alencar, S., Rebull, L., Hillendbrand, L.A. et al. 2014, AJ, 147, 34pp
Siwak, M., Rucinski, S. M., Matthews, J. M., Pojmanski, G., Kuschnig, R. et al. 2011, MNRAS, 410, 2725
Spruit H. C., Stehle R., Papaloizou J. C. B., MNRAS 1995, 275, 1223
Stauffer J. et al., 2014, AJ, 147, 34
Stone J. M., Gardiner T. A., 2007a, Phys. Fluids, 19, 4104
Stone J. M., Gardiner T. A., 2007b, ApJ, 671, 1726
van der Klis M., *Compact Stellar X-Ray Sources*, Eds. Lewin W. H. G. and van der Klis M. (Cambridge Univ. Press, Cambridge, 2006) 39
Wang, Y.-M. & Robertson, J.A. 1984, A&A, 139, 93
Wang, Y.-M. & Robertson, J.A. 1985, ApJ, 299, 85
Warner B., PASP 2004, 116, 115
Warner B., 1995, Cataclysmic variable stars, (CUP, Cambridge 1995)